

Hyperspectral monitoring of chemically sensitive plant sensors

by

Danielle A. Simmons

B.S. Rochester Institute of Technology, 2007

A thesis submitted in partial fulfillment of the
requirements for the degree of Master of Science
in the Chester F. Carlson Center for Imaging Science
College of Science
Rochester Institute of Technology

May 15, 2013

Signature of the Author _____

Accepted by _____
Coordinator, M.S. Degree Program Date

CHESTER F. CARLSON CENTER FOR IMAGING SCIENCE
ROCHESTER INSTITUTE OF TECHNOLOGY
ROCHESTER, NEW YORK

CERTIFICATE OF APPROVAL

M.S. DEGREE THESIS

The M.S. Degree Thesis of Danielle A. Simmons
has been examined and approved by the
thesis committee as satisfactory for the
thesis required for the
M.S. degree in Imaging Science

Dr. John P. Kerekes, Thesis Advisor

Date

Dr. David W. Messinger, Committee Member

Date

Dr. Carl Salvaggio, Committee Member

Date

Hyperspectral monitoring of chemically sensitive plant sensors

by

Danielle A. Simmons

Submitted to the
Chester F. Carlson Center for Imaging Science
in partial fulfillment of the requirements
for the Master of Science Degree
at the Rochester Institute of Technology

Abstract

Current events clearly demonstrate that chemical and biological threats against the public are very real. Automated detection of chemical threats is a necessary component of a system that provides early warning of an attack. Plant biologists are currently developing genetically engineered plants that de-green in the presence of explosives (i.e. TNT) in their environment. The objectives of this thesis are to study the spectral reflectance phenomenology of the plant sensors and to propose requirements for an operational monitoring system using spectral imaging technology. Hyperspectral data were collected under laboratory conditions to determine the key spectral regions in the reflectance spectra associated with the de-greening phenomenon. The collected reflectance spectra were then entered into simulated imagery created using the Rochester Institute of Technology's Digital Imaging and Remote Sensing Image Generation (DIRSIG) model. System performance was studied as a function of pixel size, radiometric noise, spectral waveband dependence and spectral resolution. It was found that a framing array sensor with 40nm wide bands centered at 645 nm, 690 nm, 875 nm, a ground sample distance of 11cm or smaller, and an signal to noise ratio of 250 or better would be sufficient for monitoring bio-sensors deployed under conditions similar to those simulated for this work.

Contents

Abstract	I
Table of Contents	II
List of Figures	V
List of Tables	IX
1 INTRODUCTION	1
1.1 OBJECTIVES	5
2 BACKGROUND-LITERATURE REVIEW	6
2.1 Bio-Sensors	6
2.2 Spectral Imaging	9
2.2.1 Spectral Imaging System Basics	9
2.2.2 Bio-sensor Monitoring Systems	11
2.3 DIRSIG	12
2.4 Band Separability	16
2.4.1 Principal Component Transform	16
2.4.2 Fisher Linear Discriminant	18

2.4.3	Angle Based Band Selection	20
3	APPROACH	23
3.1	Spectral Data Collection	24
3.2	Spectral Image Data Processing	30
3.3	DIRSIG Scene Creation	32
3.4	System Design Studies	35
3.4.1	GSD Calculation	36
3.4.2	Band Separability	37
3.4.3	Evaluation of Simulation Results	38
4	RESULTS	40
4.1	Analysis of ASD Spectra	40
4.2	Orthogonal Subspace Projection Analysis	42
4.2.1	Overview	42
4.2.2	Procedure	43
4.2.3	Results	44
4.2.4	Conclusions	48
4.3	Band Separability	49
4.4	Trade Studies	52
5	SUMMARY AND CONCLUSIONS	63
6	FUTURE WORK	65
A	ASD ANALYSIS	67
B	IDL PROGRAMS	72

<i>CONTENTS</i>	IV
C MATLAB PROGRAMS	88
REFERENCES	110

List of Figures

1.1	This figure shows an example of a setting for bio-sensors. TNT sensitive bio-sensors are planted outside of a school and are monitored by a spectral imager.	4
2.1	Example of two arabidopsis plants that were exposed to a chemical inducer and de-greened over the course of two days.	7
2.2	An Arabidopsis plant allowed to re-green for 3 days after removal of the inducer.	8
2.3	Description of FluorCam from Photon Systems Instruments.	12
2.4	(A) Plot of two spectra (B) Contour map of all band pair spectral angle.	21
3.1	Map of vapor tank layout. The inducer was a NESTT treated form of TNT.	26
3.2	Laboratory setup.	26
3.3	Petri dish used for the root to shoot experiment with a ruler for scale	27
3.4	Root to shoot collection setup	27
3.5	Vapor collection setup.	29
3.6	An image from the SOC 700.	31

3.7	Region of de-greening on bio-sensors a) SOC 700 b) FluroCam.	31
3.8	Dake Middle School entrance in MegaScene1 with trees and shrubs removed.	33
3.9	Overview of DIRSIG simulation.	34
3.10	DIRSIG images used for trade studies (a) left of entrance (b) right of entrance	34
3.11	SAM score image	38
3.12	ROC curve corresponding to SAM score image shown in Figure 3.11	39
4.1	FluorCam images of the three most responsive bio-sensors (a) Root to shoot plant 258 (b) Root to shoot plant 260 (c) Vapor plant 236	41
4.2	Root to shoot plant 258 input spectra (visible region) for OSP algorithm	45
4.3	Root to shoot plant 258 input spectra (near infrared region) for OSP algorithm	46
4.4	Root to shoot plant 260 input spectra (visible region) for OSP algorithm	46
4.5	Root to shoot plant 260 input spectra (near infrared region) for OSP algorithm	47
4.6	Vapor plant 236 input spectra (visible region) for OSP algorithm	47
4.7	Vapor plant 236 input spectra (near infrared region) for OSP algorithm	48
4.8	Input green and de-greened spectra to BAO algorithm showing bands selected by BAO algorithm	51
4.9	Area under the ROC curve surface plots for 512x512 pixels and SNR of 500	54

4.10	Area under the ROC curve surface plots for 512x512 pixels and SNR of 250	54
4.11	Area under the ROC curve surface plots for 512x512 pixels and SNR of 50	55
4.12	Area under the ROC curve surface plots for 128x128 pixels and SNR of 500	55
4.13	Area under the ROC curve surface plots for 128x128 pixels and SNR of 250	56
4.14	Area under the ROC curve surface plots for 128x128 pixels and SNR of 50	56
4.15	Area under the ROC curve surface plots for 32x32 pixels and SNR of 500	57
4.16	Area under the ROC curve surface plots for 32x32 pixels and SNR of 250	57
4.17	Area under the ROC curve surface plots for 32x32 pixels and SNR of 50	58
4.18	Areas for the left image at 128x128 pixel size for the BAO-VIS region plotted as a function of SNR	60
4.19	ROC curves for a 128x128 pixel image and a 32x32 pixel image . . .	60
4.20	The multi-spectral image, SAM image and ROC curve associated with the 128x128, BAO-vis trade study image with a bandwidth of 40 nm and an SNR of 250	62
A.1	ASD spectra of plant 236	67
A.2	ASD peak normalized spectra of plant 236	68
A.3	Spectral Angle Mapper of ASD spectra of plant 236	68

A.4	ASD spectra of plant 258	69
A.5	ASD peak normalized spectra of plant 258	69
A.6	Spectral Angle Mapper of ASD spectra of plant 258	70
A.7	ASD spectra of plant 260	70
A.8	ASD peak normalized spectra of plant 260	71
A.9	Spectral Angle Mapper of ASD spectra of plant 260	71

List of Tables

3.1	The time in Mountain Daylight Time that measurements were made of each experiment.	28
3.2	Calculated GSD for each image size	37
4.1	Summary of OSP results	49
4.2	List of wavelengths found to maximize the spectral angle between the green and de-greened spectra	50
4.3	List of wavelengths used for the BAO Full spectral subset	52
4.4	List of wavelengths used for the BAO VIS spectral subset	53
4.5	List of wavelengths used for the BAO NIR spectral subset	53

Chapter 1

INTRODUCTION

Recent global events make it clear that chemical and biological threats against the public are very real. Prevention of these threats from becoming acts is of the utmost importance to national security. There are already steps in place that serve as preventative measures. Limitations on liquids carried by passengers on planes and the presence of explosives trace detectors in airports are two examples [25]. But these types of measures are impractical and expensive for large public areas such as malls and schools. What is needed is an inexpensive method to distribute many sensors over large open areas.

Interesting progress is being made by way of engineering plant detectors. Bio-sensors are being designed to have a response that is easily recognizable by the public. One such bio-sensor has had its gene circuitry altered so that in the presence of a chemical inducer it will cease chlorophyll production and rapidly turn white [1].

Bio-sensors have been engineered to be applicable in different situations. The plants studied in this thesis have been designed to react to TNT. Another type of bio-sensor is sensitive to zinc. Depending on the situation, one type of plant could

be used to detect an explosives threat in a pedestrian area. Similarly, bio-sensors could be planted along the banks of a waterway and used to detect pollution in the water. Despite their different purposes they offer similar reactions.

Bio-sensors are ideal for use in public areas such as transportation centers, malls and schools. They require no more maintenance than the common houseplant and are easily distributed. Multiple bio-sensors could be included in the landscaping and design of a public space. Their obvious reaction to a threat would be easily seen by people in the area, however, the visible manifestations of the detection of a nefarious substance does take some time to develop.

Quick identification of a chemical attack is vital to the prevention of harm to people or property. With first generation bio-sensor technology a visible change in the plant is apparent after a day and can be remotely sensed within a couple of hours. A spectral imaging remote sensing system designed specifically for the detection of de-greening biosensors would provide the fastest indication of a threat detected by the plants. A faster response time increases the likelihood of identifying the threat and preventing it from becoming an attack. Future generations of the bio-sensor plant technology are expected to reduce the reaction time to minutes or even seconds.

Creating an effective monitoring system begins with determining what regions of the bio-sensors' spectra change over a period of exposure to an inducer. This was done in a laboratory environment using hyperspectral instruments to measure the bio-sensors' reflectance spectra. Then the significant regions of change in the spectra were identified using feature separability methods.

The Digital Imaging and Remote Sensing Image Generation (DIRSIG) simulation tool [20] was used to help determine the best combination of system parameters

to detect bio-sensor degreening. The spectra of green and de-greened bio-sensors were applied to plant models in a region of DIRSIG urban MegaScene [9]. System performance was studied as a function of pixel size, radiometric noise, spectral wave-band dependence and spectral resolution. The results are reported in this document.

As an example, Figure 1.1 shows a scenario where explosives sensitive bio-sensors would be useful. A school is shown with several bio-sensors planted around it and its walkways. To the side there is a pole on top of which sits a multi-spectral monitoring system that stares at the bio-sensors and images them. Each image is analyzed for the presence of a de-greening bio-sensor. Should the system detect de-greening, an alert would be sent to school officials or the police department for further investigation.

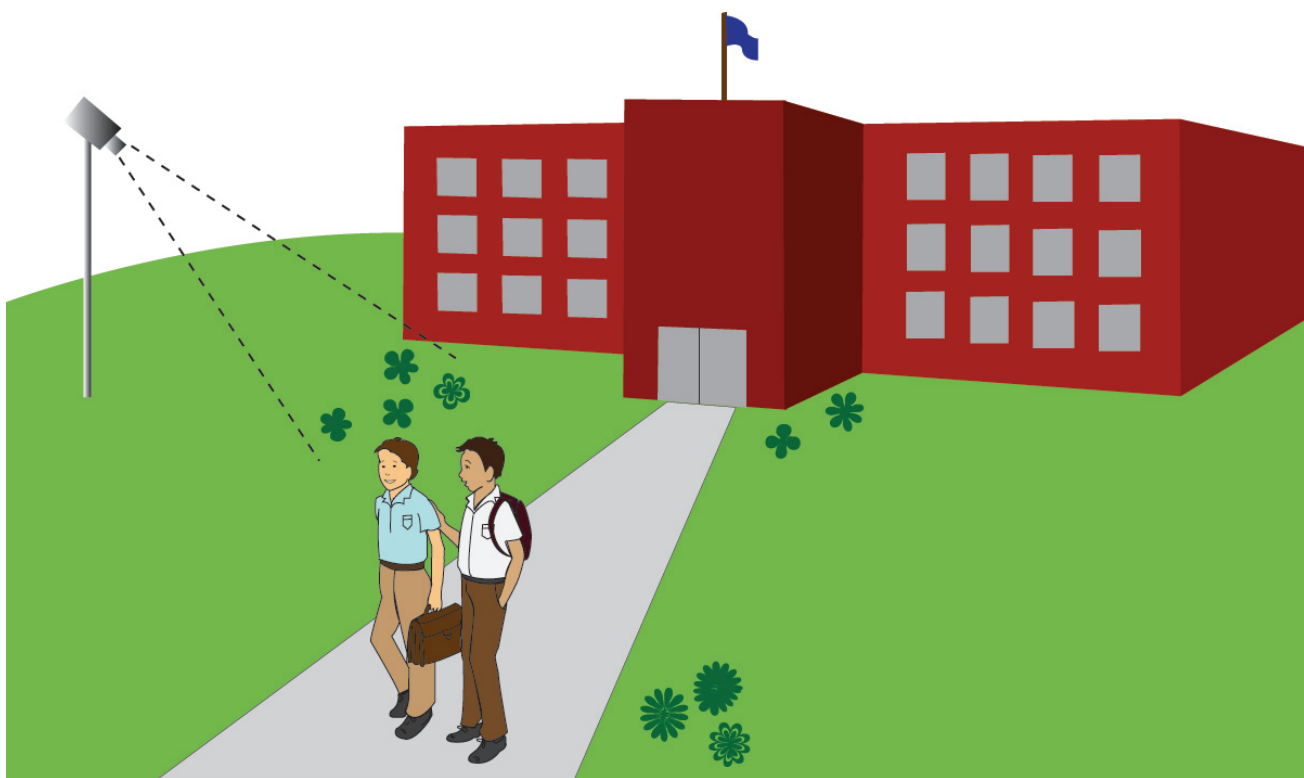


Figure 1.1: This figure shows an example of a setting for bio-sensors. TNT sensitive bio-sensors are planted outside of a school and are monitored by a spectral imager.

1.1 OBJECTIVES

The ultimate goal of this project is to make a recommendation on the type of monitoring system necessary to provide a rapid detection of de-greening in bio-sensors. This goal has been divided into three major tasks.

- **Collect hyperspectral data of bio-sensors over a period of exposure and de-greening.** Collecting spectral data of de-greening bio-sensors provided data describing the speed at which the bio-sensors de-green and what type of changes occur spectrally as the plants whiten. Data have been collected using imaging spectrometers and a spectroradiometer.
- **Analyze the collected data and determine significant features related to de-greening.** Characterizing the spectral changes that occur over the course of de-greening is imperative to the successful design of a system for monitoring bio-sensors. Once we know what spectral regions show the most change as the plant de-greens we will know where our monitoring system's detector should be the most sensitive. A band selection method was chosen to complete this task.
- **Perform trade studies on system requirements for a ground based bio-sensor monitoring system using DIRSIG.** A model of a scene similar to the one described by Figure 1.1 has been created in DIRSIG. Bio-sensor models in the scene have been attributed with spectra measured during the data collection events. Different system models will be applied to the scene to determine the best combination of requirements for early detection of de-greening. System performance was studied as a function of pixel size, radiometric noise, spectral waveband dependence and spectral resolution.

Chapter 2

BACKGROUND-LITERATURE REVIEW

2.1 Bio-Sensors

By their nature, plants are sensitive to the chemicals in the air and soil around them. Translating this sensitivity into the ability to detect specific chemical threats requires plants to have a sensing and readout (a.k.a. reporting) system.

Readout systems are commonly used by biologists to provide information about the inner workings of plants. An example of a popular reporting mechanism is fluorescence. Bio-fluorescence has become a useful indicator of biological processes in plants and animals. It occurs naturally in some types of jellyfish and coral as well as plants. Fluorescent properties may be given to plants and animals through genetic manipulation. Most often this is done through the introduction of green fluorescent protein (GFP) to the genetic makeup of the plant.

Members of the Department of Biology at Colorado State University have suc-

cessfully developed plants capable of detecting chemicals in the environment and signaling their detection through a visible readout system [1]. The bio-sensor designers felt that they must include four essential features in the readout system. First the reaction must be easily recognizable by the public. While GFP is a common reporting gene used in studies, its presence is not visible. As an alternative, the designers of the bio-sensors have created a synthetic de-greening circuit to regulate chlorophyll synthesis and degradation in the plant. The circuit is only triggered when a specific inducer is present in the plants environment. The circuit affects chlorophyll differently than normal plant senesce, thereby preventing the de-greening from being mistaken for poor plant health. Figure 2.1 shows images of two plants as they de-greened over the course of two days.

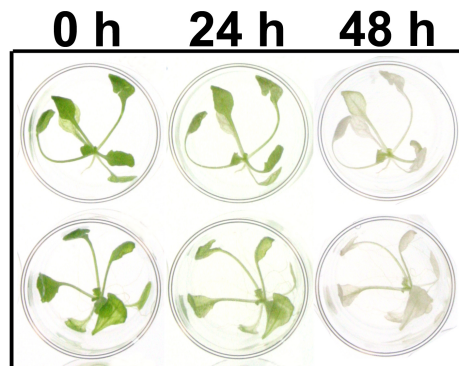


Figure 2.1: Example of two arabidopsis plants that were exposed to a chemical inducer and de-greened over the course of two days.

The second feature desirable in the reporting system of the bio-sensor is that the reaction shown by the plant should be detectable remotely. From Figure 2.1 it is obvious that the degreening phenomena is detectable remotely via a color camera. One of the objectives of this project is to monitor the de-greening process with a

hyperspectral instrument and quantify the change that occurs.

A rapid response to an inducer is the third key feature desired in the readout system of the bio-sensor. In first generation plants, complete degreening has been shown to occur within 24 to 48 hours. Changes were remotely detectable at 2 hours post exposure. Future generations will hopefully show even faster response times.

A reset capacity is the final feature desired in the readout system. It allows the same plant to be used for multiple detections. Figure 2.2 shows a plant allowed to re-green for 3 days after the removal of the inducer. In order for re-greening to begin, the inducer must be completely removed from the plant's system.



Figure 2.2: An Arabidopsis plant allowed to re-green for 3 days after removal of the inducer.

The plants studied in the project are sensitive to inducers via two methods. The first method is through their root system. Contaminated water or soil that comes into contact with the root system triggers de-greening. This method is most useful in detecting environmental pollution (i.e. zinc pollution) or buried explosives (i.e. TNT). The second type of bio-sensor is sensitive to inducers in the air. Exposed via chemical vapors, these plants would be most useful in public areas. Hypothetically,

should a chemical threat pass a bio-sensor, it would be able to detect the chemical by way of the vapor that passed over it.

This study will focus on the use of spectral imaging to remotely detect changes in the bio-sensors as de-greening occurs. A better understanding of the bio-sensors behavior allows for a better understanding of the phenomenology found in our data. Two data collection events occurred during this study and both methods of exposure were used.

2.2 Spectral Imaging

The goal of this thesis is to make recommendations about the design of a spectral imager for the monitoring of bio-sensors. A general understanding of spectral imagers is needed before a discussion of specific requirements may take place. The systems discussed here will be restricted to the visible to near infrared portion of the electromagnetic spectrum due to their relevance to this thesis. In this chapter a brief overview of the main components of multispectral imaging instruments is provided. Then some vegetation monitoring systems are described to illustrate the type of system that might be developed for this project.

2.2.1 Spectral Imaging System Basics

Spectral imagers collect data in three dimensions. Spatial data is recorded in two dimensions and spectral data is recorded in a third. The many different types of spectral imagers can be easily described by the methods they use to collect spatial and spectral data [21]. The following is an overview of those methods.

Spatial data is collected by either scanning or staring. Scanning instruments

are generally divided into two types. A whiskbroom instrument has a single spot FOV that scans in two dimensions (i.e. along and across track). Alternatively, a pushbroom scanner has a slit aperture that exposes a line of detectors to create one spatial dimension while movement of the instrument gathers data across the second spatial dimension. Staring instruments do not require movement. Instead they employ a 2D array of detectors that are exposed simultaneously [19].

Spectral imagers can also be classified by the way that they capture spectral data. In general they are either filtering, dispersive or interferometric imagers [21]. Filter based systems place a filter in the optical path of the sensor. A common design for these types of systems places the filters on a mounted wheel that rotates. Then an image is captured through each one as the wheel turns. Tunable filters are electrically adjustable filters that are placed directly over detector elements. There are two types of tunable filters, liquid crystal filters and acusto-optical filters [8]. Both are electronically adjustable methods to generate interference with incident energy. Spectral imagers with dispersive systems use prisms and/or gratings to separate the incoming light into different spectral components that can then be measured by the detectors [22]. The third method used to collect spectral data is interferometry. Interferometric systems separate a beam into different paths (of different lengths) and recombine them. The resulting interference controls the strength of the response on the detector [7]. One of these methods is paired with a spatial sampling method to create a spectral imager. For the sake of simplicity this thesis will focus on array detectors that utilize filters.

2.2.2 Bio-sensor Monitoring Systems

Accurately sensing the reactions of a bio-sensor is paramount to using it as an indicator. The de-greening response is a completely unique type of readout system. Understanding systems designed for bio-sensors with different types of readout systems will assist in developing an approach for the design of a de-greening bio-sensor monitoring system.

In the case of GFP readout systems this type of fluorescence can be easily distinguished from natural plant fluorescence in bio-sensors. One method uses laser induced fluorescence systems to excite the fluorescence response and CCD cameras to measure it [11]. In one such system the camera sensor is responsive in the 400 nm to 900 nm region. Images were collected at 420 nm, 480 nm, 510 nm and 550 nm using a filter wheel placed in front of the camera. The image captured through the 510 nm filter isolated the GFP fluorescence from the natural plant fluorescence features that occurred above and below it in the reflectance spectra. Similar active systems have been created for sensing of these types of bio-sensors [15] [16] [23] [13].

Plant stress is often quantified by fluorescence imaging as well. Chlorophyll is naturally fluorescent and causes plants to be mildly fluorescent. Chlorophyll fluorescence occurs when the plant receives more light than it requires to conduct photosynthesis. The plant relieves itself of the extra energy through fluorescence [17]. Generally, when the plant is healthy and working at a high photosynthetic rate the amount of chlorophyll fluorescence is low. When the plant begins to feel stress from over stimulation by a light source or other changes in its environment it will start to fluoresce more [26].

Instruments such as the FluorCam sold by Photo Systems Instruments [10] are lab based fluorescence imagers. Figure 2.3 shows the inside of the imager which is

a closed box. Each unit is customized to the purchaser's needs but in general have similar components. LED's are used to create excitation energy and measurement light. Then there is a filter wheel with four to eight filters (again, depending on the users needs) that sits in front of a CCD camera. The detector in the camera is sensitive in the 400 to 1000 nm wavelength range. Example imagery from this system is shown later in this proposal. This type of instrument is useful in the lab environment when using small plants or parts of plants. It is impractical for large field deployed bio-sensors.

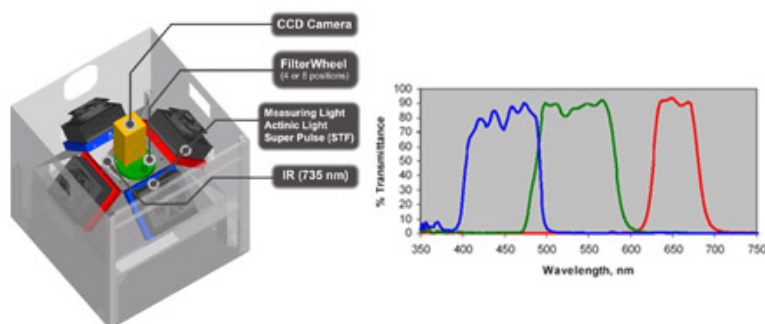


Figure 2.3: Description of FluorCam from Photon Systems Instruments.

2.3 DIRSIG

This project employed the synthetic image generation tool called Digital Imaging and Remote Sensing Image Generation (DIRSIG) developed at RIT [20]. First, a scene was created to represent field deployment of bio-sensors. Different sensor system designs were then tested to determine the system requirements of an imager needed to monitor the biosensors. Presented here is a brief overview of DIRSIG and

its many uses.

DIRSIG is a collection of first principles based radiation propagation sub models [2]. It produces simulated imagery in the visible through thermal regions of the electromagnetic spectrum. DIRSIG as a whole incorporates several models that consider things such as surface BRDF characteristics, transmission and atmospheric conditions (i.e. MODTRAN). These models allow the software to fully recreate the imaging chain from source to scene to sensor and produce radiance information in the final imagery.

An overly simplified description of DIRSIG would be to call it ray tracing software. It rigorously accounts for the interactions of energy from its source to the sensor. Along this path, DIRSIG records interactions with surfaces that the energy encounters. Reflection, transmission and absorption events are accounted. A radiometry sub model computes incident radiance from the traced path [20].

The radiance information is augmented by a model of the sensor and the platform it sits on. DIRSIG allows the user to model several types of sensors such as whiskbroom, line scanner and framing array. The sensitivity of the sensor and its geometric makeup influence the recorded radiance information. Platform modeling tells DIRSIG how the sensor is positioned in the scene. The platform can either be static, as in the case of framing arrays. Or, in the case where temporal sampling is responsible for creating a second spatial dimension (i.e. scanning systems) the platform can be dynamic. Either way, information is provided by the user describing the sensors location and orientation with respect to the scene.

DIRSIG's thoroughness in modeling the image chain from end to end makes it a versatile tool. It is useful for testing system designs, algorithm testing, algorithm training and analyst training. For system designers the rigorous radiometry model

included in DIRSIG allows the user to judge the performance of a prototyped system in terms of its output imagery. For algorithm training, DIRSIG can produce a signature space in which the algorithm designer can expect the target to occupy. Then the designer can constrain the algorithm to this space and limit false alarms [2]. Testing algorithms on simulated imagery gives the advantage of knowing exactly what is in the imagery. DIRSIG also allows the designer to create a set of test images varying in scene content, atmospheric conditions and time of collection to test the algorithm. Analyst training on DIRSIG imagery provides the option of creating imagery that represents scenes of interest for which there is no imagery available. These uses are often employed in conjunction with one another.

The first step towards creating a DIRSIG simulation is to create the scene with which it will interact. Creating an entirely new scene for DIRSIG is a complicated process. Literally, a scene must be built from the ground up. A great deal of data must be collected to create an accurate representation of an area. Information such as area elevation maps, texture maps, material properties, and scene details need to be captured and modeled. The general construction process is laid out in the DIRSIG Users Manual. The following is a modified excerpt from the manual summarizing scene construction in twelve steps [2].

1. Identify area to model. The scene to be constructed may be a real area or it may be a fictional location. If the candidate scene is a real scene, it is helpful to acquire ground and overhead imagery of the area to help construct features.
2. Locate or generate terrain data for the area. For real scenes, this may be in the form of a U.S.G.S. Digital Elevation Model (DEM). For a fictional scene, this could imply “designing” the general terrain and features that it will include.

3. Create a facet model of the terrain. This might entail using a triangular irregular network (TIN) generation program that can process a digital elevation model. For a fictional scene, it might imply hand creating a terrain that matches the desired features of the proposed scene.
4. Construct 3D models of the various objects in the scene. This would include houses, trees, buildings, vehicles, etc. This can be accomplished in a variety of Computer Aided Design (CAD) applications.
5. Acquire the necessary material thermodynamic and optical properties for the objects in the scene. This includes acquiring spectral reflectance and emissivity curves (or reusing data from other DIRSIG scenes). Spectral data from other sources will need to be converted to the appropriate DIRSIG file.
6. Create a DIRSIG Material Database File for your scene. If the scene is similar to an existing scene, the Material Database File for that scene can be used as a base. In some cases, a duplicate copy material database from another scene can be used.
7. Create a material map for the scene. This is an optional but powerful technique that can be used to attribute the facetized terrain. If aerial imagery is available, it might be used as an input to terrain classification algorithm.
8. Import and attribute the CAD objects using the Bulldozer tool. When the model is attributed, it is saved as a Geometric Database (GDB) File.
9. Create any texture maps that can be used to drive in-material spatial-spectral variation.

10. Use the Bulldozer tool to place the attributed objects (GDB files) onto face-sized terrain.
11. Create a DIRSIG configuration file to simulate a sensor imaging your scene.
12. Run the DIRSIG simulation and review the generated imagery.

For this project biosensor models were added to an existing scene. The focus of the work lies in using DIRSIG simulated imagery for testing the effects of different system parameters on the detection of de-greened bio-sensors.

2.4 Band Separability

The spectrometers used in the collection phase of this project collect data in hundreds of channels over the range of the visible to near infrared region of the spectrum. Ideally, this level of detail will help determine the specific spectral regions of interest pertaining to the de-greening phenomena. Most likely, the change in the spectrum will be isolated to one or two smaller regions of the spectrum than what is measured. Determining what bands show change over the course of de-greening is essential to the design of the monitoring system. This will help simplify the design, reduce the amount of redundant information collected and save in computational costs when detection algorithms are used on the imagery from the system. Several separability methods are explored in the following sections.

2.4.1 Principal Component Transform

The Principal component (PC) transform is a linear transformation that decorrelates the data and maximizes the representation of variability in a reduced dimensionality

space [19]. The new space has the benefit of each axis being orthogonal to the others. As a result, the first image in a PC transform contains the most variability; the second image contains the second most and so on to the point where most of the remaining bands appear to be noise. The noisy images could be ignored and the high information bands could be used for image classification, thereby reducing the computation complexity of the task [18].

PC transformation begins with the eigenvectors and eigenvalues of the image covariance matrix. In an image with k bands and a digital count (DC) in each band we can define a transformed space of k bands as $PC = E^T x$ where x is a spectral vector, PC is the vector in the principal component space and E is a matrix of eigenvectors.

$$\mathbf{PC} = \begin{pmatrix} PC_1 \\ PC_2 \\ \vdots \\ PC_k \end{pmatrix} \quad (2.1)$$

$$\mathbf{E} = \begin{pmatrix} e_{11} & e_{21} & \dots & e_{k1} \\ e_{12} & e_{22} & \dots & e_{k2} \\ \vdots & \vdots & \ddots & \vdots \\ e_{1k} & e_{2k} & \dots & e_{kk} \end{pmatrix} \quad (2.2)$$

While the PC transform is a simple and valuable tool, it holds two drawbacks for use in this project. First, it is based on global image statistics. The regions of de-greened vegetation may be very small compared to the size of the image. Therefore the de-greened regions could be ignored in the transform calculation. Second, the first PC band of one scene may highlight different information than the first PC band

of another scene. As a result, it would be hard to relate the presence of de-greening in a scene to another.

2.4.2 Fisher Linear Discriminant

The spectra of the green bio-sensors will be similar to the de-greened spectra. To assist in discriminating between these two classes we now take a look at Fishers linear discriminant. The goal of this separability method is to reduce a d -dimensional space down to a one dimensional problem. Essentially, this methods searches for a line in d -space on which to project the data that will produce the greatest separability between the two classes [4].

Consider a set of d -dimensional samples $x_1 \dots, x_n$. A linear combination of \mathbf{x} creates the scalar dot product

$$\mathbf{y} = \mathbf{w}^T \mathbf{x}. \quad (2.3)$$

The elements of \mathbf{y} can also be interpreted as the projection of each \mathbf{x}_i onto \mathbf{w} . Our goal is to find \mathbf{w} such that the separation between the classes is maximized. Here enters Fisher's linear discriminant. By finding the \mathbf{w} that maximizes equation 2.4 we find the \mathbf{w} that maximizes the separation between classes.

$$J(w) = \frac{|\tilde{m}_1 - \tilde{m}_2|^2}{\tilde{s}_1^2 - \tilde{s}_2^2} \quad (2.4)$$

The d -dimension sample mean is defined as

$$\tilde{\mathbf{m}}_i = \frac{1}{n_i} \sum_{\mathbf{x} \in D_i} \mathbf{x} \quad (2.5)$$

Therefore the sample mean for the projected points used in equation 2.4 is defined as

$$\tilde{m}_i = \mathbf{w}^t \mathbf{m}_i \quad (2.6)$$

The variables \tilde{s}_1^2 and \tilde{s}_2^2 represent the scatter in each projected class. Their sum is equal to the total within-class scatter. If we begin by defining the scatter matrices as

$$\mathbf{S}_i = \sum_{\mathbf{x} \in \mathbf{D}_i} (\mathbf{x} - \mathbf{m}_i)(\mathbf{x} - \mathbf{m}_i)^T \quad (2.7)$$

Where their sum equals

$$\mathbf{S}_w = \mathbf{S}_1 + \mathbf{S}_2 \quad (2.8)$$

Then the scatters used in equation 2.4 may be written as

$$\begin{aligned} \tilde{s}_i^2 &= \sum_{y \in Y_i} (y - \tilde{m}_i)^2 \\ &= \sum_{\mathbf{x} \in D_i} (\mathbf{w}^T \mathbf{x} - \mathbf{w}^T \mathbf{m}_i)^2 \\ &= \sum_{\mathbf{x} \in D_i} \mathbf{w}^T (\mathbf{x} - \mathbf{m}_i)(\mathbf{x} - \mathbf{m}_i)^T \mathbf{w} \\ &= \mathbf{w}^T \mathbf{S}_i \mathbf{w} \end{aligned} \quad (2.9)$$

with the sum

$$\tilde{s}_1^2 + \tilde{s}_2^2 = \mathbf{w}^T \mathbf{S}_w \mathbf{w} \quad (2.10)$$

Similarly, we may write the difference in projected means as

$$(\tilde{m}_1 - \tilde{m}_2)^2 = (\mathbf{w}^T \mathbf{m}_1 - \mathbf{w}^T \mathbf{m}_2)^2$$

$$\begin{aligned}
&= \mathbf{w}^T(\mathbf{m}_1 - \mathbf{m}_2)(\mathbf{m}_1 - \mathbf{m}_2)^T \mathbf{w} \\
&= \mathbf{w}^T \mathbf{S}_B \mathbf{w}
\end{aligned} \tag{2.11}$$

where

$$\mathbf{S}_B = (\mathbf{m}_1 - \mathbf{m}_2)(\mathbf{m}_1 - \mathbf{m}_2)^T. \tag{2.12}$$

Equations 2.11 and 2.10 allow us to rewrite the Fisher linear discriminant as

$$\mathbf{J}(\mathbf{w}) = \frac{\mathbf{w}^T \mathbf{S}_B \mathbf{w}}{\mathbf{w}^T \mathbf{S}_w \mathbf{w}} \tag{2.13}$$

A vector \mathbf{w} that maximizes equation 2.13 is

$$\mathbf{w} = \mathbf{S}_w^{-1}(\mathbf{m}_1 - \mathbf{m}_2). \tag{2.14}$$

The Fisher linear discriminant helps describe a space where the separation between the green and de-greened spectra of the biosensors is maximized. We can compute \mathbf{w} for a green and de-greened spectra to find a space to project the spectra onto that highlights their differences. But transforming the imagery into a new space would be challenging.

2.4.3 Angle Based Band Selection

Keshava developed a Spectral Angle Mapper (SAM) optimization method that improves algorithm performance by reducing data dimensionality [12]. The technique iteratively adds bands that create a maximum increase in spectral angle until additions begin to decrease the angle. In other words, it adds bands until additions are no longer able to increase the spectral angle.

Spectral angle mapper quantifies the angular separation of two spectral vectors. For two spectral vectors \mathbf{x} and \mathbf{y} of length m , it is defined as

$$\theta(\mathbf{x}, \mathbf{y}) = \arccos \left(\frac{\langle \mathbf{x}, \mathbf{y} \rangle}{\|\mathbf{x}\| \|\mathbf{y}\|} \right). \quad (2.15)$$

The analysis begins by calculating the spectral angle between every band pair combination. The band pair corresponding to either the minimum or the maximum spectral angle can be used as the starting point for the iterative band add-on (BAO) technique. Figure 2.4 shows a plot of two spectra and a contour map of the spectral angle for all possible band pairs.

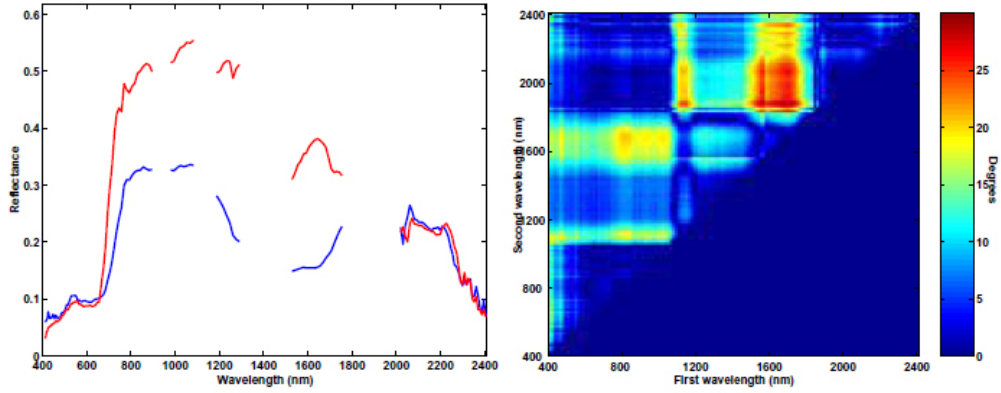


Figure 2.4: (A) Plot of two spectra (B) Contour map of all band pair spectral angle.

From the chosen starting point the following decomposition of SAM is used for the BAO technique. Again, x and y are two spectral vectors of length k that have been partitioned such that $\mathbf{x} = [\mathbf{x}_a \ \mathbf{x}_b]$ and $\mathbf{y} = [\mathbf{y}_a \ \mathbf{y}_b]$ where $k = a + b$.

$$\cos \theta(\mathbf{x}, \mathbf{y}) = \left(\frac{\langle \mathbf{x}, \mathbf{y} \rangle}{\|\mathbf{x}\| \|\mathbf{y}\|} \right) \quad (2.16)$$

$$= \cos \theta_a \frac{1 + \frac{\langle x_b, y_b \rangle}{\langle x_a, y_a \rangle}}{\sqrt{1 + \frac{\|x_b\|^2}{\|x_a\|^2}} \sqrt{1 + \frac{\|y_b\|^2}{\|y_a\|^2}}} \quad (2.17)$$

$$= \cos \theta_a \beta \quad (2.18)$$

Using equation 2.18, β is calculated for all remaining bands based on the initial pair of bands. The procedure is repeated until no bands satisfy $\beta \geq 1$. The user now has a set of bands that create a maximum spectral angle.

This method was employed to determine the meaningful bands in the bio-sensor degreening process. In comparison to Fisher's Linear Discriminate and the PC transform it has the advantage of not transforming the data into a new space. It also works with as few as one sample from each class.

Chapter 3

APPROACH

The ultimate objective of this work is to be able to make a recommendation about the best type of sensor parameters to use for monitoring bio-sensors. This objective was divided into three tasks in Section 1.1. First, collect data of the bio-sensors de-greening. Second, characterize the spectral changes that occur. And lastly, based on the collected data, start designing a system to detect de-greening.

This chapter expands on each task by describing the approach used to complete them. First, the collection procedure used for the August 2008 and September 2009 events is described. Next a discussion of the application of the band add-on method described in the background literature review is presented. The remaining sections describe designing the DIRSIG scene, modeling the bio-sensors, and conducting the trade studies. The last section in this chapter discusses the methods used to evaluate the performance of the system models.

3.1 Spectral Data Collection

The bio-sensor's de-greening readout system was specifically chosen because it is a visible phenomenon. De-greening plants are readily apparent to the human eye, as opposed to a fluorescence or infrared response. This reaction has also proven to be detectable by remote sensing instrumentation before a visible change is apparent [1]. Remote detection saves valuable time that can be used for executing a response to the detected threat.

The first step towards monitoring bio-sensors and detecting a reaction to a threat is to gather spectral data of the de-greening bio-sensors. Characterizing the spectral changes that occur during de-greening will allow for earlier detection of triggered bio-sensor and assist in the design of a monitoring system.

A collection was held in August 2008 in Dr. June Medford's lab at Colorado State University. The following methodology was used to make the measurements of the biosensors.

An Analytical Spectral Devices (ASD) FieldSpec 3 was used to make measurements of the plant sentinels. The ASD samples from 350-2500 nm with a 1.4 nm sampling interval from 350-1000 nm and a 2 nm sampling interval from 1000-2500 nm [5]. The fiber optic was placed in the pistol grip with the 1° foreoptic. The instrument was set to average 10 spectra per file and 3 files were collected for each measurement made.

Four types of tobacco plants were measured during this collect. One set of plants was exposed to TNT via particulates in the air. These plants are henceforth referred to as the vapor plants. The other set of plants were exposed via their root system (a.k.a. root to shoot plants). For each method of exposure there were both bio-sensors and wild-type (unaltered) tobacco plants. The wild-type plants were

experimental controls.

The vapor plants were grown in soil in individual pots and arranged in two 20 gallon aquariums. Fifteen plants (mixed bio-sensors and control plants) were placed in a tank with a red rim. This tank was the experimental tank exposed to the inducer. For this experiment a non-hazardous explosive for security training and testing (NESTT) treated form of TNT was used to induce de-greening [14]. The inducer will be referred to as TNT in the remainder of the document. The eleven other plants (both bio-sensors and controls) were placed in a green rimmed tank that served as the control tank and was not exposed to TNT. The control tank also contained a data logger (a.k.a. the HOBO) to monitor the temperature and humidity levels, as well as a Spectralon white reference standard used for calibrating the ASD. Both tanks were sealed after the TNT was placed in the red-rimmed tank. Inside the tank, the plants were organized similarly to the layout shown in Figure 3.1. The plant names beginning with sr1- are the wild type control plants. The three digit numbers represent bio-sensor plants.

The collection setup was built around the experiment setup shown in Figure 3.2. In the experiment setup there was an 8 ft sawhorse with a sodium vapor lamp suspended from it. The lamp provided the necessary growing illumination for the plants. Shown beneath the lamp are the two aquariums. We centered our collection around this setup in hopes of reducing stress on the plants. Excessive movement could have caused some of the plants, the TNT, the HOBO or the white reference to fall over.

The root to shoot experiment is so called because of the method used to expose the plants to TNT. Figure 3.3 is a photograph of a Petri dish containing three wild type tobacco plants. The plants are exposed to TNT via the agar they were rooted

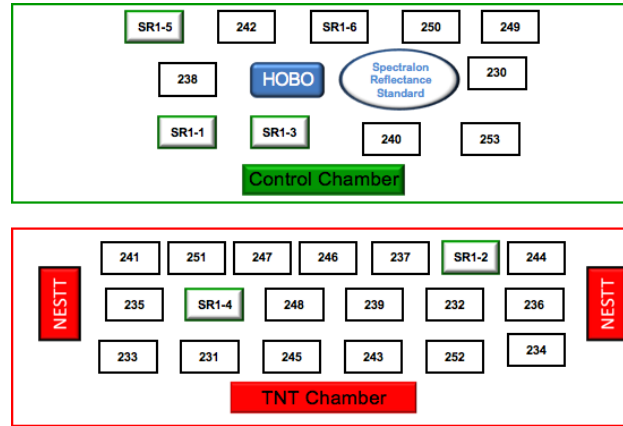


Figure 3.1: Map of vapor tank layout. The inducer was a NESTT treated form of TNT.



Figure 3.2: Laboratory setup.

in. These plants are only one-quarter to one-half of an inch in size.

Figure 3.4 shows the setup used to measure the root to shoot experiment. Since the agar was transparent the dishes were placed over the white reference while making measurements with the ASD. The lids to the Petri dishes were removed during

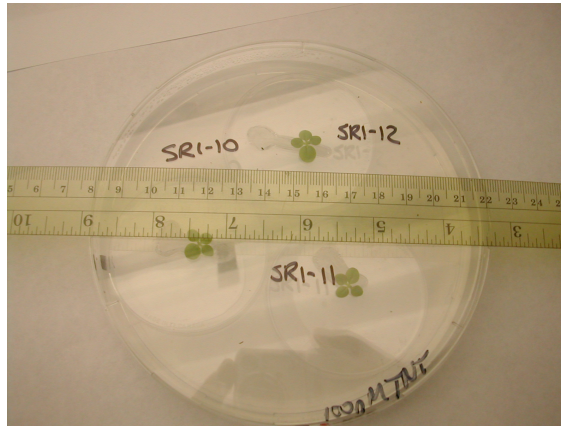


Figure 3.3: Petri dish used for the root to shoot experiment with a ruler for scale

collection. Exposure to the labs relatively dry air (compared to the environment inside the closed Petri dish) was limited as much as possible since differences in humidity could have been stressful for the plants. When not being measured, the lids were replaced on the dishes and positioned under growth lights.

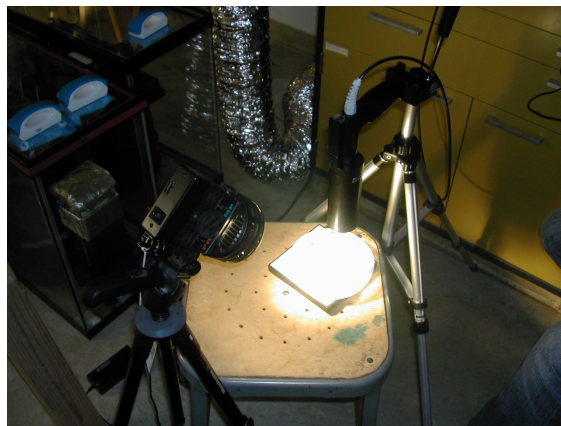


Figure 3.4: Root to shoot collection setup

A second sawhorse is visible to the left of the first sawhorse in Figure 3.2. Secured

to the top of the sawhorse are two SOC instruments used by our research partner Dr. Arnab Shaw from Gitam Technologies. The SOC 700 collects spectral images between 390 to 900 nm with approximately 4 nm resolution. The SOC 720 collects spectral images in the region from 900 to 1700 nm at approximately 9 nm resolution. Both instruments generate images that are 640 by 640 pixels in size. Typically one tank would be imaged under the SOC instruments while the plants in the remaining tank were measured with the ASD.

Measurement of the plants began after the TNT was placed in the red rimmed tank on August 5th at 1500 hours. First the vapor control tank was measured, followed by the vapor TNT tank, and then the root to shoot plants. The root to shoot plants consisted of two different experiments. The first experiment was exposed to TNT on Sunday, August 3rd at 1000 hours. The second set of plants was exposed at 1500 hours on August 5th. Measurements were repeated every six hours until August 7th at 1500 hours with the exception that no overnight measurements were made. See also, Table 3.1.

	Experiment Sampling						
	5-Aug-08		6-Aug-08			7-Aug-08	
	1500 MDT	2100 MDT	900 MDT	1500 MDT	2100 MDT	900 MDT	1500 MDT
3-Aug-08 R2S	x		x	x	x	x	x
5-Aug-08 R2S	x	x	x	x	x	x	x
5-Aug-08 Vapor	x	x	x	x	x	x	x

Table 3.1: The time in Mountain Daylight Time that measurements were made of each experiment.

The overhead fluorescent lights and the growth lamp were shut off during measurement of the plants. Plants in the tanks were illuminated with a single full spectrum light that was repositioned for each plant. The ASD fore optic was mounted on a tripod that was also repositioned to measure each plant. A photograph of the

ASD, lighting and tank setup may be seen in Figure 3.5.



Figure 3.5: Vapor collection setup.

The vapor control tank was always measured before the vapor TNT tank. The ASD was optimized and a white reference was collected from the Spectralon panel first. Then the plants were measured. An effort was made to re-measure the white reference and optimize the ASD before moving onto the TNT tank.

For the root to shoot measurements the ASD and illumination source were in fixed positions relative to the Spectralon panel on the stool. The ASD was optimized before the first measurement and periodically there-after to account for drift in the instrument. The Petri dishes were placed on top of the Spectralon and positioned under the foreoptic one at a time (see Figure 3.4). The plate was rotated to the next plant until all three plants in the dish had been measured.

Many of the plants that were measured were too small to fill the field of view (FOV) of the ASD foreoptic. Without the aid of a targeting device it was difficult to determine if the plant being measured was accurately placed in the FOV. Watching the spectrum change on the ASD laptop screen helped refine the targeting of the

fore-optic on both the tank and root to shoot plants. Adjustments were made until the spectrum seemed to be the most vegetation-like possible.

A second collection event occurred during the first week of September of 2009. There are some notable differences between the second event and the previous one. Based on lessons learned from the previous collection (see Section 4.1) the ASD was not used. Also, this event only made measurements of plants exposed via their root system. These plants included controls and bio-sensors like the previous study. Additionally, bio-sensors were included that had been exposed to agents to simulate common stressors felt by plants in uncontrolled (i.e. non-laboratory) environments. The goal was to determine if the bio-sensors' stress reactions are distinguishable from a TNT induced reaction. Mannitol was used to prevent water absorption and simulate draught conditions. Another set was exposed to a slightly acidic environment. A third set was exposed to higher than normal levels of phosphorus to simulate over fertilization. The spectra collected from the stressed plants are included in DIRSIG simulations.

Despite the fore mentioned differences, the collection procedure was similar to the one described for the August 2008 collection. The same measurement schedule was followed. Also, the SOC setup and measurement procedure was the same.

3.2 Spectral Image Data Processing

The spectral images from the SOC instruments needed to be processed to be able to extract spectral reflectance data. First the images were converted from digital number to spectral reflectance. Then spectral vectors were sampled from the imagery for use in the creation of the DIRSIG scene.

Figure 3.6 is a three band representation of a spectral image collected by the SOC

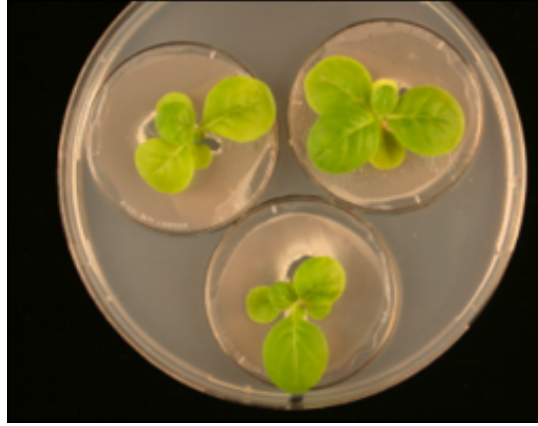


Figure 3.6: An image from the SOC 700.

700. All other images collected for this experiment also contained a white reference. The data processing began by converting the image to spectral reflectance. A 10 by 10 pixel area of the white reference was selected from the image and an average spectral vector was calculated. The entire image was divided by the average white reference spectral vector to create a spectral reflectance image.

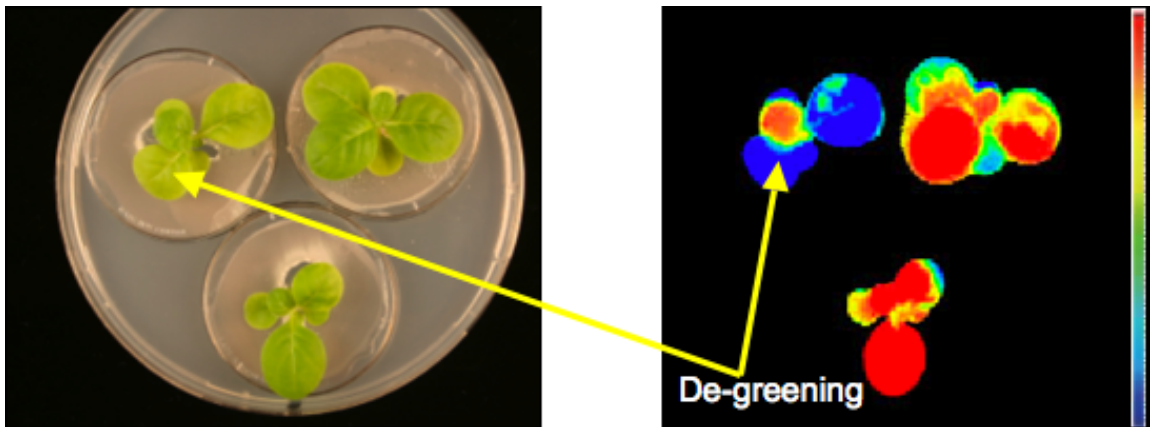


Figure 3.7: Region of de-greening on bio-sensors a) SOC 700 b) FluroCam.

FluroCam imagery and recommendations by Dr. Medford's lab were used to select regions of de-greening in the SOC reflectance images. Figure 3.7 compares a de-greened region in a SOC 700 image and a FluroCam image. A sample of roughly 30 spectral pixels was selected from the de-greened region. In some cases, depending on the size of the de-greened region in the image, the sample size was less. An average of the selected vectors was computed to reduce the presence of noise in the resulting spectral vector. At this point the vectors were ready for use in the DIRSIG scene.

3.3 DIRSIG Scene Creation

The DIRSIG scene created for this project meets two criteria. First, the scene depicts a plausible setting for bio-sensors to be applied. Second, 3D models of the bio-sensors are added to the scene and attributed with reflectance spectra gathered during the data collections.

This project took advantage of an existing DIRSIG scene. MegaScene1 covers a portion of the Greater Rochester area of New York State. Within this scene we modified the region around Duke Middle School to meet our needs. The focus is around the entrance to the school where bio-sensors would be the most useful for detecting explosives threats before they entered the school. While work has been done to alter the scene's content, a great deal of work was saved by starting with an existing scene.

Changes to the scene aimed to simplify the area and allow room for adding models of bio-sensors. Extra trees and shrubbery were removed from the scene resulting in Figure 3.8. Models of the bio-sensors were created, attributed and placed in the scene following the procedure described in Section 2.3. Lastly, shrubbery and textures were

added to refine the scene. Figure 3.9 shows an overview of the completed scene.



Figure 3.8: Dake Middle School entrance in MegaScene1 with trees and shrubs removed.

The scene shown in Figure 3.9 was divided into two smaller images for the trade studies. In Figure 3.10 we see the two images depicting either side of the building entrance. The DIRSIG bio-sensor models were attributed with spectra collected during the August 2009 collection. The plants in the left image represent change in a biosensor after exposure. The leftmost plant is 48 hours after exposure, second from the left is 24 hours after, the third plant is 12 hours, the fourth plant is 6 hours after and the last plant in the image is at the time of exposure. The right image shows a green biosensor (i.e. a biosensor at the time of exposure), a pH stressed biosensor, a draught stressed bio-sensor, an over fertilized bio-sensor and a degreened bio-sensor.



Figure 3.9: Overview of DIRSIG simulation.

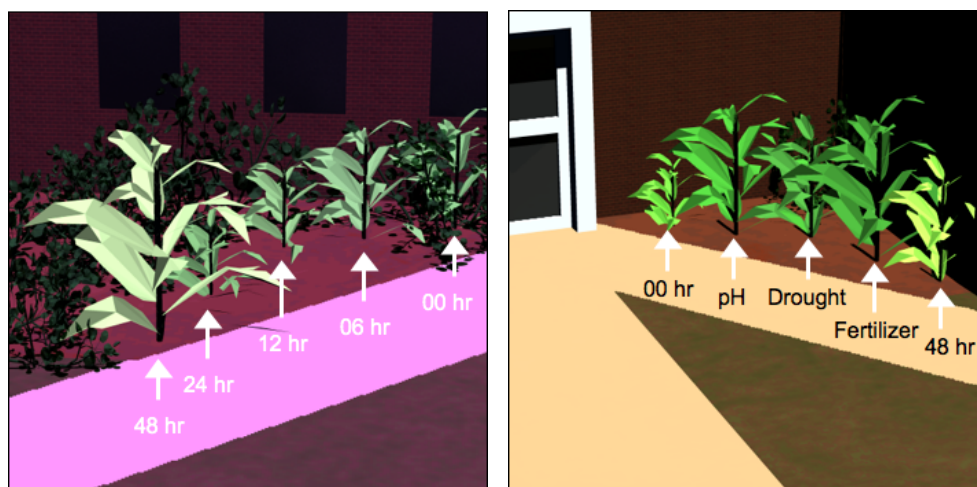


Figure 3.10: DIRSIG images used for trade studies (a) left of entrance (b) right of entrance

3.4 System Design Studies

Trade studies were performed to determine what the best combination of system parameters are for a bio-sensor monitoring system. There are many components that could be considered in the creation of the system. We begin with the assumption that the system will be a mounted focal plane array. The following parameters were tested.

- Spectral Region and Band Selection
 - 400 nm to 1700 nm
 - 400 nm to 1700 nm of BAO suggested regions
 - 400 nm to 900 nm of BAO suggested regions
 - 900 nm to 1700 nm of BAO suggested regions
- Spectral resolution of the sensor
 - 5 nm bandwidth
 - 10 nm bandwidth
 - 40 nm bandwidth
 - 160 nm bandwidth
- Ground sample distance (GSD) as indicated by image size (see Table 3.2)
 - 512 x 512 pixels
 - 128 x 128 pixels
 - 32 x 32 pixels

- Signal to noise ratio (SNR)
 - 500
 - 250
 - 50

IDL code or ENVI functions were used to create the images within the trade space. The spectral resolution of the sensor was adjusted using a RECT function passed over the spectral dimension of the images. The images were downsampled using ENVI's *PixelAggregate* option. Finally, uniform noise was added to the images assuming Gaussian statistics. Relevant code may be found in Appendix B

In total, 144 images were created (for each image, left or right) to cover the range of system parameters described above. Different GSD's were simulated by using down-sampled versions of the original image. The trade space could be expanded beyond the one shown to include field of view, focal length and other sensor parameters that effect GSD. The method used serves as a starting point. In future studies, an additional trade study looking at the factors affecting GSD should be conducted.

3.4.1 GSD Calculation

The GSD at the center of the three image sizes was calculated using the input provided to DIRSIG to generate the 512 by 512 pixel scene. GSD is calculated as

$$GSD = \frac{pR}{f \cos \theta} \quad (3.1)$$

where p is the pixel pitch of the detector, R is the range from sensor to the target, f is the focal length of the system and θ is the look angle between the target and

system. Table 3.2 lists the calculated GSD for each image size of the left and right image.

	Left Scene	Right Scene
512 by 512	2.6 cm	2.8 cm
128 by 128	10.4 cm	11 cm
32 by 32	41.4 cm	44 cm

Table 3.2: Calculated GSD for each image size

3.4.2 Band Separability

The angle based band selection method discussed in Section 2.4.3 shows the most promise for clearly detailing what regions of the bio-sensor's spectra show change over the course of degreening. This method was implemented in Matlab and applied to the spectral reflectance vectors selected from the August 2009 SOC imagery. The inputs to the algorithm are a green spectrum and a de-greened spectrum. The algorithm evaluates all band pairs and adds bands that increase the spectral angle until an increase is no longer possible. The bands of interest provided by this algorithm were used to determine the sensitivity of the monitoring system.

A starting point for the sensor sensitivity and spectral resolution was provided by the band-selection algorithm results. The number of bands suggested by the algorithm and the location of those bands will suggest where the sensor needs to be the most sensitive to changes. The range that the sensor covers depends on the range of the selected bands.

3.4.3 Evaluation of Simulation Results

Using simulated imagery provides the advantage of knowing the exact location of green and de-greened bio-sensors. This makes the evaluation of the results from the system easier and more accurate. Spectral Angle Mapper (SAM) was used to compare green and de-greened spectra in the image. A review of SAM was provided in Section 2.4.3. The algorithm was implemented in MATLAB. A single band SAM image was created for each trade study image. The SAM image contained a spectral angle for every pixel in the image. Figure 3.11 is a SAM score image where lighter pixels indicate a closer match.



Figure 3.11: SAM score image

The score image was then compared to the truth data created by DIRSIG to make a Receiver Operator Characteristic (ROC) curve for each image. Figure 3.12 is the ROC curve for the score image shown in Figure 3.11. The Area Under the Curve (AUC) for each ROC curve was calculated and surface plots were created to compare the performance of the trade study images.

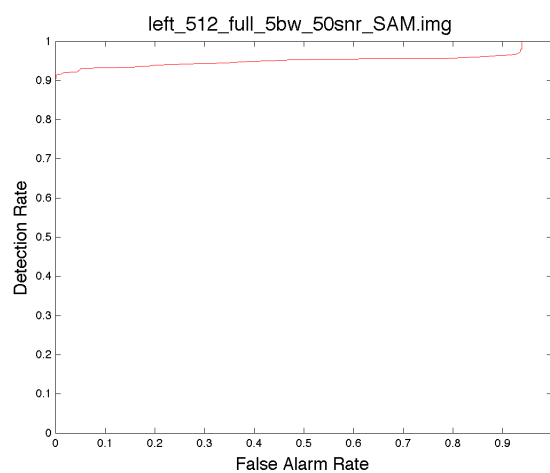


Figure 3.12: ROC curve corresponding to SAM score image shown in Figure 3.11

Chapter 4

RESULTS

This sections presents the results from this project. It begins with the analysis of the ASD data collected in August of 2008. Next is a review of the orthogonal subspace projection analysis performed on the ASD data using additional information taken from the SOC instruments data. Then the results of the BAO algorithm on the data collected in September 2009 are presented. The final section of this chapter discusses the trade studies and makes a recommendation based on the results.

4.1 Analysis of ASD Spectra

First the ASD data files were converted to ASCII files using ASDs ViewSpecPro software. From the ASCII files a single text file was made for each plant that contained all of the reflectance spectra collected for that plant ordered from the initial to the final measurement. A text file was also made for each plant holding the peak normalized spectra for each measurement. Finally, the spectral angle between the initial measurement and each subsequent measurement was calculated

and printed out to a text file. All of the data was entered into Excel spreadsheets and graphed. Three bio-sensor plants showed a de-greening reaction during the August 2008 data collection. The blue regions in the Figure 4.1 FluorCam images are regions of stress in the plants, indicating a reaction to the inducer. These three plants are focused on in the analysis.

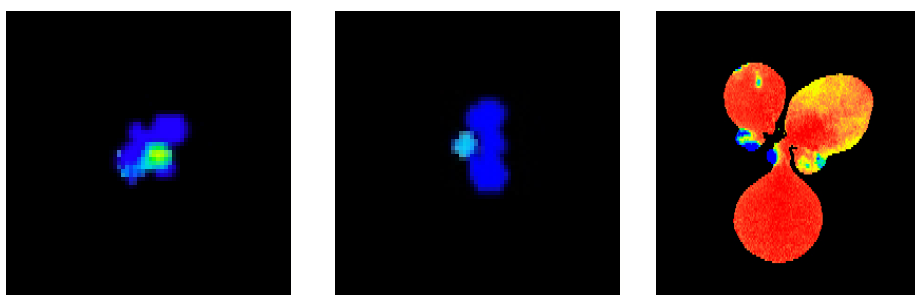


Figure 4.1: FluorCam images of the three most responsive bio-sensors (a) Root to shoot plant 258 (b) Root to shoot plant 260 (c) Vapor plant 236

Plots of each plant spectrum can be found in Appendix A. Also in Appendix A is a plot of spectral angle over time. Ultimately, these graphs proved to be inconclusive. Plants 258 and 260 have very little vegetative shape in the visible region due to how small they were in comparison to the field of view of the collection instrument. Nor do the plots for plant 236 show a consistent change over time. This is most likely due to the small region of the plant that showed a reaction in comparison to the rest of the plant.

4.2 Orthogonal Subspace Projection Analysis

A challenge faced by using the ASD data is the sub-pixel size of the plants measured. The ASD has a single instantaneous field of view and the plants were significantly smaller than it. Therefore background materials such as soil, agar and green leaves were also measured along with the plant. Orthogonal subspace projection (OSP) was then used to determine the abundance of the de-greened plant spectrum in the mixed pixel measured by the ASD.

4.2.1 Overview

Consider a scene containing k distinct end members called v_{lk} . The linear mixture model assumes that all observed spectra from said scene are a linear combination of the pure end members v . For each band $(1, 2, 3 \dots l)$ in the scene a pixel may be represented as

$$\begin{aligned}
 x_1 &= v_{11}f_1 + v_{12}f_2 \dots + v_{1k}f_k + \varepsilon_1 \\
 x_2 &= v_{21}f_1 + v_{22}f_2 \dots + v_{2k}f_k + \varepsilon_2 \\
 &\vdots \\
 x_l &= v_{l1}f_1 + v_{l2}f_2 \dots + v_{lk}f_k + \varepsilon_l
 \end{aligned} \tag{4.1}$$

where f represents the fractional abundance of each end member in the pixel. The final term ε represents the residual error in the mixture model [19].

As mentioned before, the ASD has a single instantaneous field of view. Any items that fell within its field of view were combined into a single pixel that is assumed to follow a linear mixture model. One method for determining the fractional abundance

of the de-greened spectra in the mixed pixel is through use of OSP. The normalized OSP estimates the abundance of a target spectrum t in a test spectrum x . First, OSP uses a projection operator P_b^\perp to reduce the presence of the background constituents discussed above. Then the algorithm applies a matched filter to search for similarities to the target spectrum (de-greened spectrum from SOC image) in the test spectrum (ASD spectra) [19].

$$\overline{T}_{OSP}(X) = \frac{t^T P_b^\perp x}{t^T P_b^\perp t} \quad (4.2)$$

Additional analysis has taken place to determine if the spectra of a de-greened bio-sensor is present in the ASD data. Our research partner Gitam was able to identify differences in the spectra of a de-greened plant using the data from the imaging spectrometers they used. It is this data that has been used to define the target and basis vectors for input into a normalized OSP algorithm.

4.2.2 Procedure

For this analysis the abundance of de-greened spectra in the ASD measurement of a bio-sensor at the end of the exposure period was calculated using OSP. The de-greened plant target spectra were selected from the SOC image cubes based on the regions highlighted in blue in Figure 4.1. Background endmembers were collected from the same hyperspectral images. They include the gel medium the root to shoot plants where growing in, the soil the vapor plant was potted in and samples of green vegetation. A green sample was not taken for root to shoot plants 258 and 260 since the FluorCam image indicates that there are not green regions. Each OSP calculation reflects the abundance of the de-greened SOC spectra in the ASD spectrum when given a certain set of background spectra.

The instrument used by RIT to collect spectra is significantly different from the instruments Gitam used. The RIT instrument (ASD) collects a single spectrum per measurement. The measurement covers the range from 350 to 2500 nm at one nanometer resolution. Gitam used two imaging spectrometers to cover a smaller region of the spectrum. The SOC 700 collects between 390 to 900 nm with approximately 4 nm resolution. The SOC 720 collects in the region from 900 to 1700 nm at approximately 9 nm resolution. Both instruments generate images that are 640 by 640 pixels in size.

It was necessary to convert the SOC data to reflectance units. Samples, 6 by 6 pixels in size, were selected from the white reference panels in the SOC imagery. An average of the spectra in the selected region was computed. The selected end member spectra from the SOC imagery were then divided by the averaged white reference spectrum to create spectra in reflectance units.

The spectral vectors supplied to the OSP algorithm must have the same number of bands and represent the same regions of the spectrum. Regions of the ASD spectra were selected to match the VIS and NIR regions covered by the two SOC instruments. The subsets were down sampled to match the resolution of the SOC data using an averaging kernel. Once the ASD data mimicked the spectral resolution and range of the SOC data, it was used as the test vector, t , in the OSP algorithm.

4.2.3 Results

This section presents plots of the spectra that were supplied to each run of the normalized OSP algorithm. The target vector is the de-green spectrum that the fractional abundance is calculated from. This spectrum comes from the SOC data (as do the gel, green plant and soil basis vectors). The test vector is the mixed

spectrum from the ASD. The fractional abundance of the target vector in the test vector is reported with the plot.

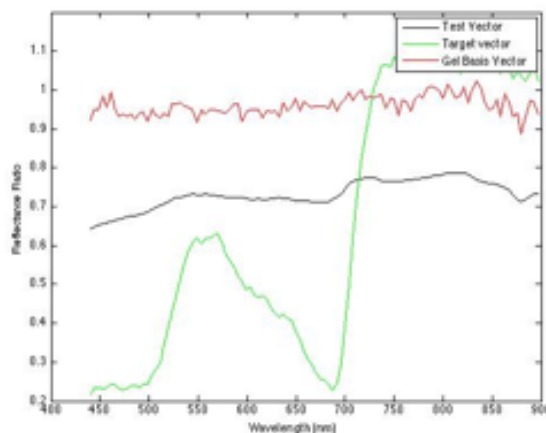


Figure 4.2: Root to shoot plant 258 input spectra (visible region) for OSP algorithm

From visual inspection of the Figure 4.2 it is easy to see that the test spectrum more closely resemble the gel basis spectrum than the target de-greened plant spectrum. One explanation for this is the large field of view of the ASD in comparison to the size of the plant being measured. The OSP algorithm calculated a 0.06 fractional abundance of the target spectrum in the test spectrum.

Figure 4.3 shows the inputs for near infrared region of the spectrum of plant 258. The OSP algorithm calculated a 0.36 fractional abundance of the target vector in the test vector. The higher abundance may be because the gel and target vector share a very similar spectral shape.

The OSP algorithm run for root to shoot plant 260 had very similar visible region input spectra to the spectra shown for root to shoot plant 258 (see Figures 4.2 and 4.4). A 0.11 fractional abundance of the target vector was found in the test vector.

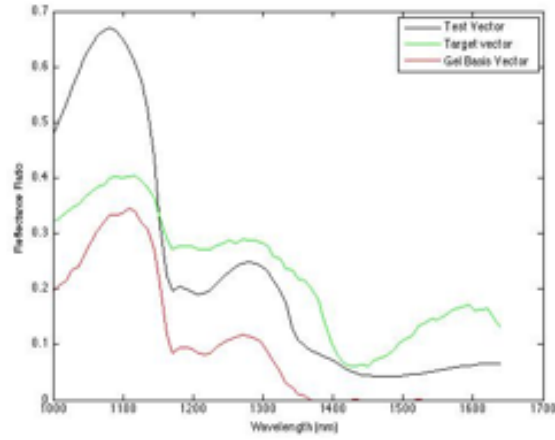


Figure 4.3: Root to shoot plant 258 input spectra (near infrared region) for OSP algorithm

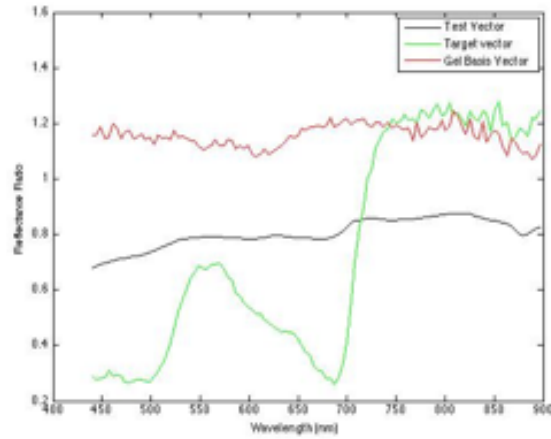


Figure 4.4: Root to shoot plant 260 input spectra (visible region) for OSP algorithm

As shown in Figure 4.5, the inputs shown for the NIR region of plant 260 are similar to the inputs for plant 258. A 0.15 fractional abundance of the de-greened

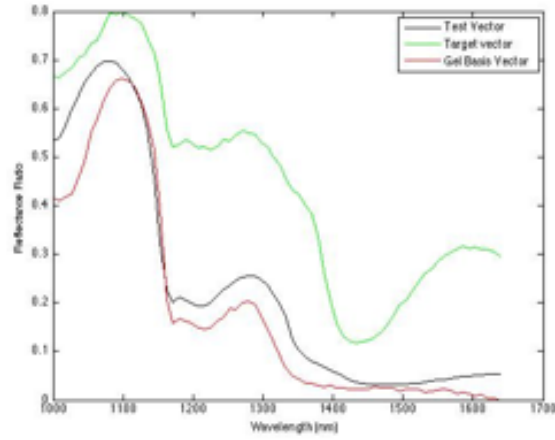


Figure 4.5: Root to shoot plant 260 input spectra (near infrared region) for OSP algorithm

plant spectra was found in the ASD test spectra.

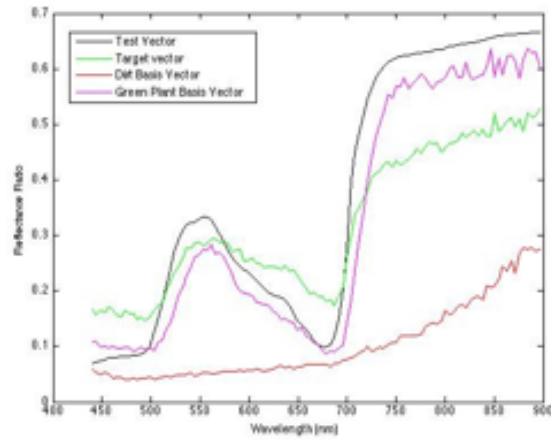


Figure 4.6: Vapor plant 236 input spectra (visible region) for OSP algorithm

Figure 4.6 shows the spectra used for the OSP calculation in the visible region

of the spectra for plant 236. The fractional abundance of degreened data in vapor plant 236 was calculated to be 0.75. Plant 236 was much larger than plant 258 or 260 and occupied a larger portion of the FOV of the ASD. Therefore the test spectrum in this case most likely contain more vegetation than in the previous two cases.

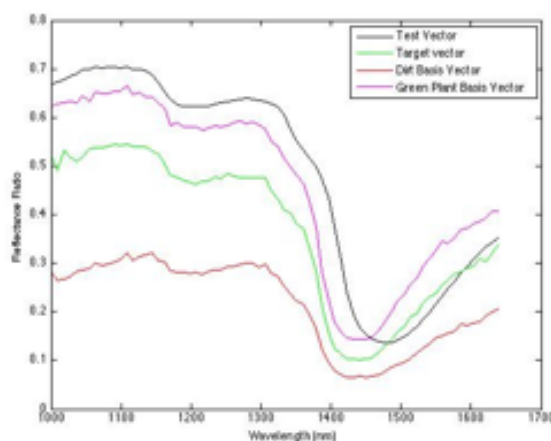


Figure 4.7: Vapor plant 236 input spectra (near infrared region) for OSP algorithm

The spectral inputs to the OSP calculation for Vapor plant 236 in the NIR region are shown in Figure 4.7. A 0.81 fractional abundance of the de-greened plant spectra was found in the test spectra.

4.2.4 Conclusions

Table 4.1 summarizes the results of this analysis. The results show the highest abundance of the de-greened spectra in vapor plant 236. This result may be contributed to the size of the vapor plants. The vapor plants were larger than the root to shoot plants. Therefore they filled a larger portion of the ASD's FOV than the root to

shoot plants and causing a stronger contribution to the recorded spectrum. The loss of red-edge detail in the root to shoot spectra agrees with the conclusion that they were too small to measure.

Normalized OSP: Fractional Abundance		
	VIS	NIR
R2S Plant 258	0.06	0.36
R2S Plant 260	0.11	0.15
Vapor Plant 236	0.75	0.81

Table 4.1: Summary of OSP results

Based on the difficulties caused by the large FOV of the instrument (compared to the relatively small area showing a reaction on the bio-sensors) it was determined that the reaction shown by the bio-sensors could not be accurately measured by the ASD. Issues with ASD's FOV have been well documented. Even if the plants were large enough to fill the FOV of the ASD's foreoptic the reacting area might still be too small to be accurately measured. Issues with the randomization of the ASD's fiber optic cable are well documented [6] [24].

4.3 Band Separability

Results using the band add on technique described in Section 2.4.3 found the bands listed in Table 4.2 to maximize the spectral angle between the two classes. Figure 4.8 shows the input spectra to the algorithm. These results indicate where the detector must be sensitive in order to differentiate between a green and de-greened bio-sensor.

SOC 700	SOC 720
625 nm	1070 nm
630 nm	1410 nm
635 nm	1420 nm
650 nm	1445 nm
665 nm	1635 nm
670 nm	1645 nm
675 nm	
680 nm	
685 nm	
690 nm	
695 nm	
700 nm	
875 nm	

Table 4.2: List of wavelengths found to maximize the spectral angle between the green and de-greened spectra

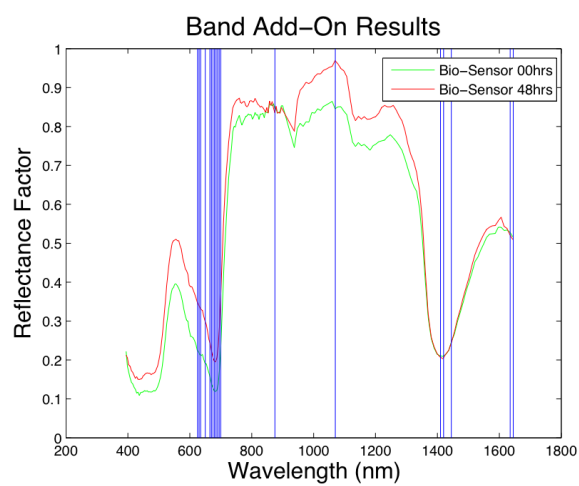


Figure 4.8: Input green and de-greened spectra to BAO algorithm showing bands selected by BAO algorithm

4.4 Trade Studies

The purpose of these trade studies is to be able to make recommendations about the type of system needed to accurately monitor bio-sensors. Figures 4.9 thru 4.17 are surface plots of the area under the ROC curve for each of the 144 trade study images. Each plot represents an image size (i.e. GSD) and SNR combination. The left plot corresponds to the left image and the right plot corresponds to the right image. The plot axes, x, y, and z are the spectral bandwidth, spectral region subset and the area respectively. An explanation of the BAO spectral subsets is described in Tables 4.3 to 4.5. Also, the "Full" subset denotes the complete spectral range from 400 nm to 1700 nm sampled according to bandwidth.

BAO Full

10 nm	40 nm	160 nm
630	645	570
650	690	735
665	875	875
680	1070	1135
695	1415	1485
875	1640	1650
1070		
1415		
1445		
1640		

Table 4.3: List of wavelengths used for the BAO Full spectral subset

BAO VIS

10 nm	40 nm	160 nm
630	645	570
650	690	735
665	875	875
680		
695		
875		

Table 4.4: List of wavelengths used for the BAO VIS spectral subset

BAO NIR

10 nm	40 nm	160 nm
1070	1070	1135
1415	1415	1485
1445	1640	1650
1640		

Table 4.5: List of wavelengths used for the BAO NIR spectral subset

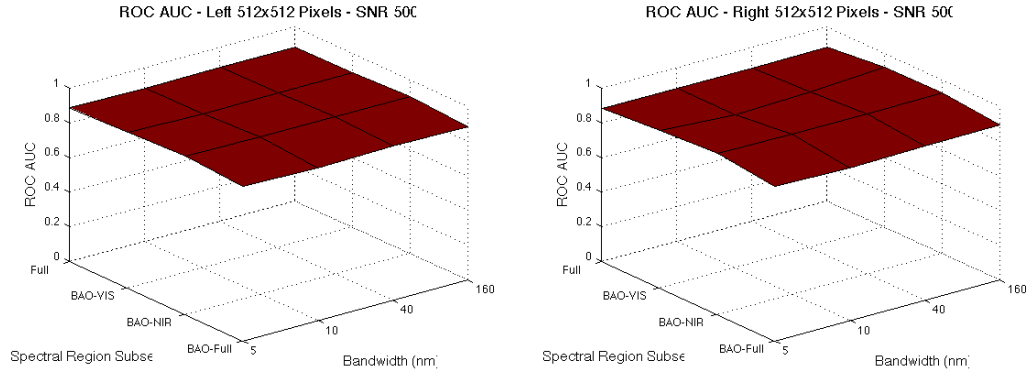


Figure 4.9: Area under the ROC curve surface plots for 512x512 pixels and SNR of 500

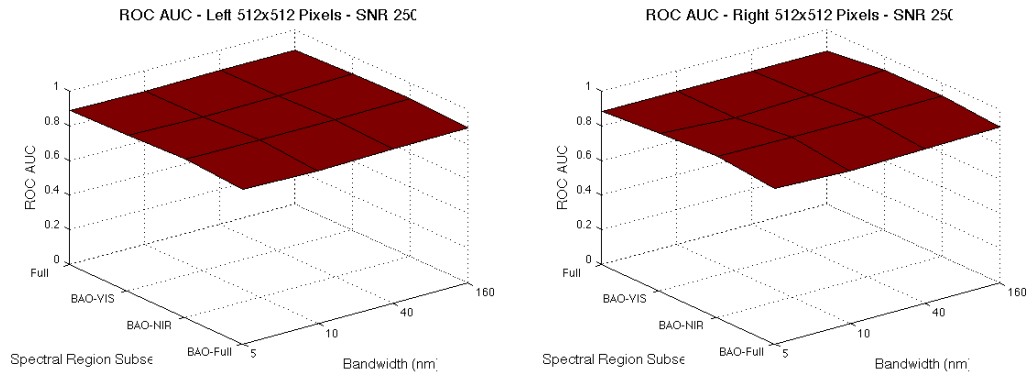


Figure 4.10: Area under the ROC curve surface plots for 512x512 pixels and SNR of 250

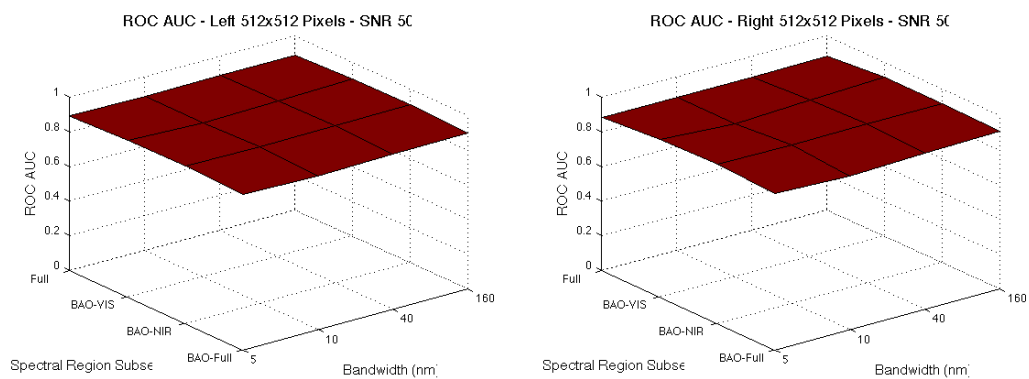


Figure 4.11: Area under the ROC curve surface plots for 512x512 pixels and SNR of 50

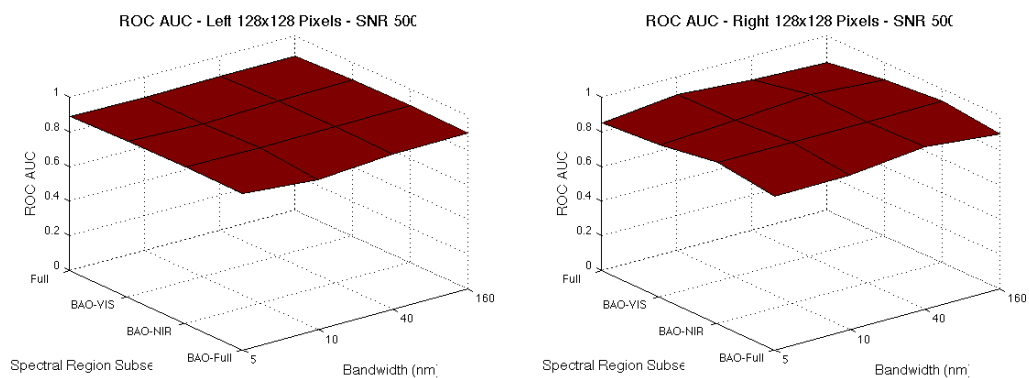


Figure 4.12: Area under the ROC curve surface plots for 128x128 pixels and SNR of 500

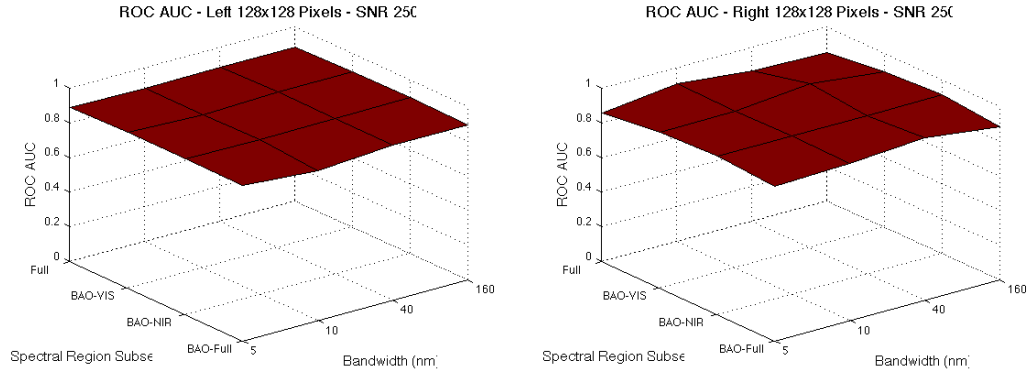


Figure 4.13: Area under the ROC curve surface plots for 128x128 pixels and SNR of 250

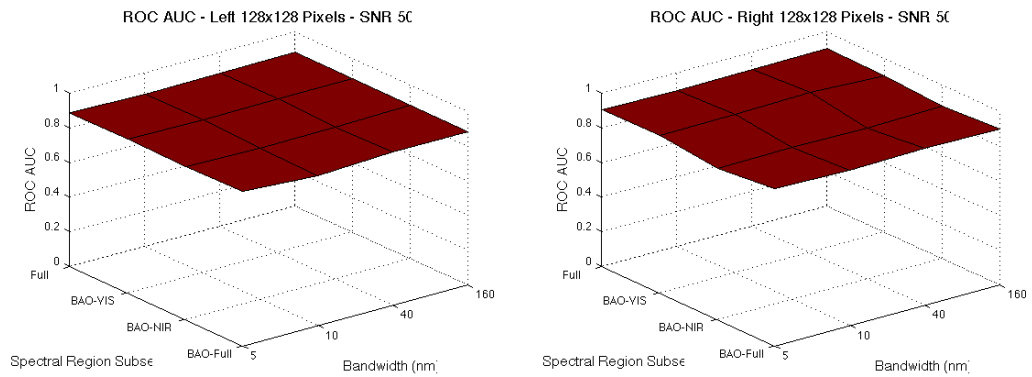


Figure 4.14: Area under the ROC curve surface plots for 128x128 pixels and SNR of 50

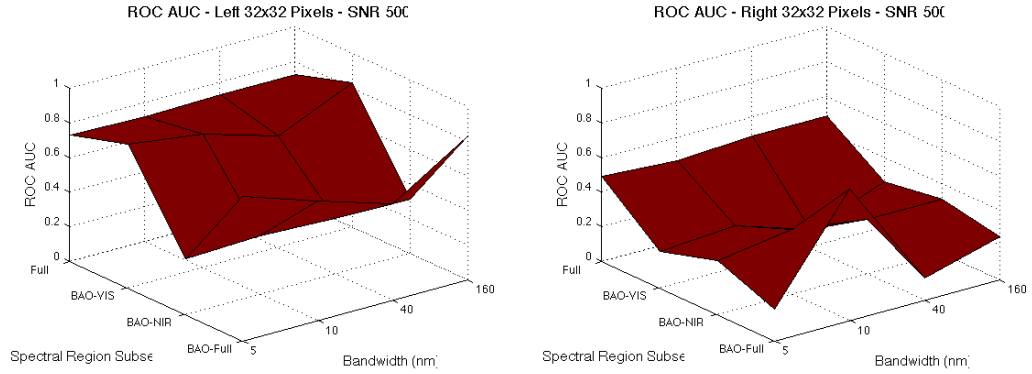


Figure 4.15: Area under the ROC curve surface plots for 32x32 pixels and SNR of 500

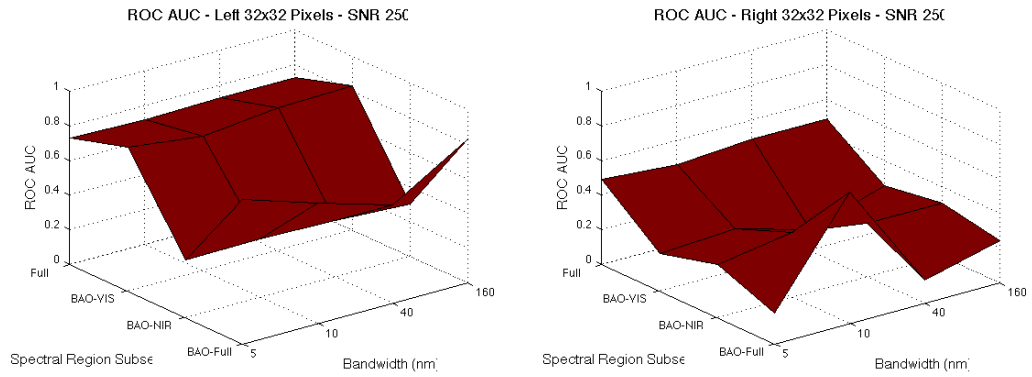


Figure 4.16: Area under the ROC curve surface plots for 32x32 pixels and SNR of 250

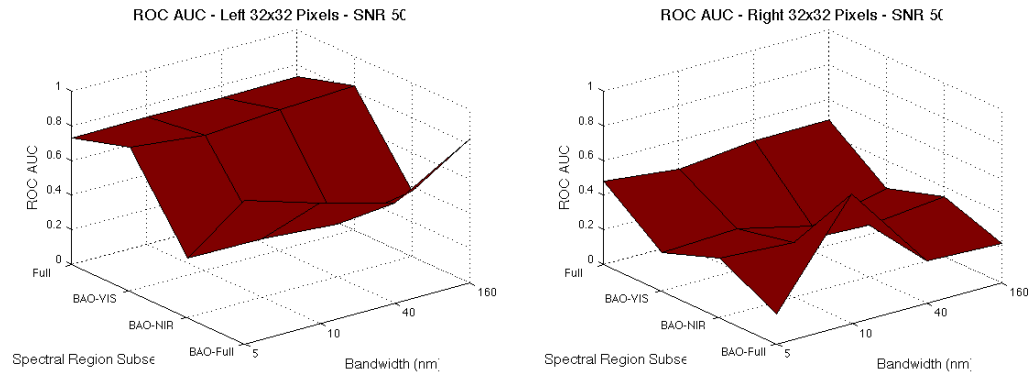


Figure 4.17: Area under the ROC curve surface plots for 32x32 pixels and SNR of 50

A qualitative review of the plots leads to a couple of observations. First, some obvious trends that you would expect to see are appearing in the data. As the image size and SNR decrease, so does the area under the curve. In other words, as noise increases and spatial resolution declines, the quality of the data decreases, making it harder to accurately detect the target. Another noticeable trend is the decrease in ROC curve area as you move down the ‘bandwidth’ axis.

The AUC for the 512x512 pixel images is comparable to that of the 128x128 pixel images. It is only when the resolution is further reduced in the 32x32 pixel image that a noticeable change in response to noise, bandwidth and spectral region may be found.

The surface plots indicate that the BAO technique was successful. Across all image sizes and SNR levels, the BAO-Full and BAO-VIS band selections performed better than the Full spectrum with only a few exceptions. This suggests that a silicon based detector should be sufficient for detecting changes in bio-sensors.

The SNR levels do not appear to have a significant impact on the ROC curves. For example, the areas for the left image at 128x128 pixel size(i.e. 10.36 cm GSD) for the BAO-VIS region are plotted as a function of SNR in Figure 4.18. The areas vary little across the changing SNR values. Most of the change in this data set is caused by the change in bandwidth.

The greatest decrease in ROC curve area is due to the change in GSD via change in image size. The area under the ROC curve decreased by approximately 0.2 from the 128x128 pixel to the 32x32 pixel images step down in image size. The 128x128 pixel image performs well compared to the 32x32 images. The detection rate is much greater than that achieved by the 32x32 images (see Figure 4.19).

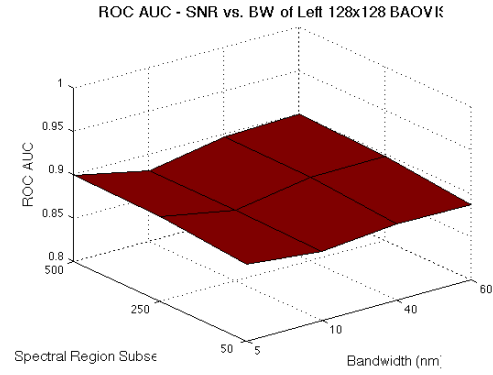


Figure 4.18: Areas for the left image at 128x128 pixel size for the BAO-VIS region plotted as a function of SNR

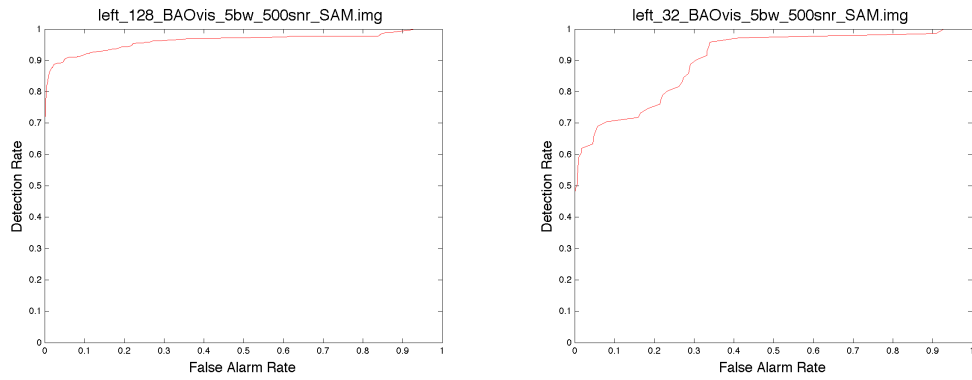


Figure 4.19: ROC curves for a 128x128 pixel image and a 32x32 pixel image

Based on this analysis it is recommended that the following parameters from the trade study would be adequate for detecting bio-sensor de-greening.

- A GSD of 11 cm or better (this GSD is represented in the 128 x 128 pixel image)
- Three 40 nm wide bands centered at 645 nm, 690 nm and 875 nm (the BAO-vis regions)
- An SNR of 250 or better
- A framing array sensor

Figure 4.20 shows the image, the SAM image, and the ROC curve for the trade study parameters represented by this recommendation.

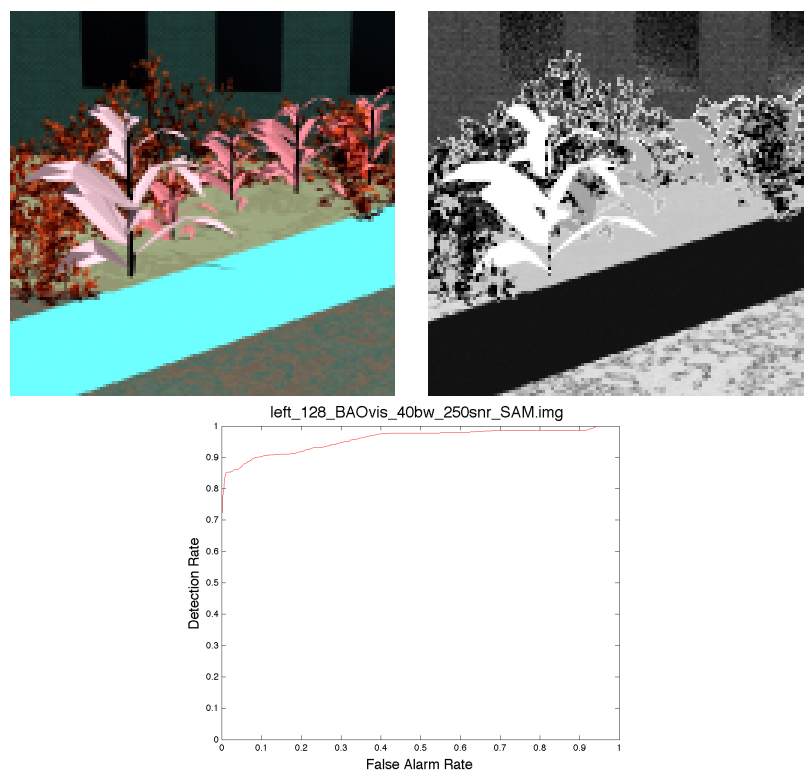


Figure 4.20: The multi-spectral image, SAM image and ROC curve associated with the 128x128, BAO-vis trade study image with a bandwidth of 40 nm and an SNR of 250

Chapter 5

SUMMARY AND CONCLUSIONS

This document reviewed the task of monitoring de-greening bio-sensors as proposed. Background information was provided on monitoring other types of bio-sensors. Chlorophyll and GFP fluorescence measurement systems were reviewed. A detailed discussion of the creation of de-greening bio-sensors was provided. Then tools used in the completion of this task were described including DIRSIG and several band separability methods. Next, the approach taken for completing this task was reviewed and the data collection process was described. Modifications to an existing DIRSIG scene were discussed.

Next, the approach for designing a system was detailed, discussing the application of the results from the angle-based band selection. It was found that a framing array sensor with 40nm wide bands centered at 645 nm, 690 nm, 875 nm, a ground sample distance of 11cm or smaller, and an signal to noise ratio of 250 or better would be sufficient for monitoring bio-sensors deployed under conditions similar to

those simulated for this work.

Some challenges complicated the measurement and analysis procedures used. The plants were small relative to the FOV of the instruments used to measure their spectra. They were also quite sensitive to atmospheric changes caused by frequent handling. The success of a real-world monitoring system partially depends on future generations of bio-sensors being larger and more hardy.

Chapter 6

FUTURE WORK

This thesis laid out a process to follow for the modeling of a multi-spectral bio-sensor monitoring system. A recommendation on system requirements was made, but more work could be done to refine this recommendation and further understand the phenomenology of the plants. This chapter outlines work that lies outside of the scope of this thesis.

A somewhat simplified approach was taken to modeling a bio-sensor imaging system. The focus was held on four parameters: GSD, SNR, spectral resolution and bandwidth. Additional work should be done to refine the GSD parameter. GSD is impacted by several factors such as FOV, sensor size. Another set of trade studies could be done working within the recommendations from this work to determine what system parameters best produce the recommended 11 cm GSD.

Another avenue to investigate is the effects of different illumination conditions on detection of the bio-sensors. DIRSIG is the perfect tool to use to answer the question: How does the time of day and weather conditions effect bio-sensor detection?

Additional work could also be done to investigate the phenomenological differ-

ences between stressed bio-sensors and de-greening bio-sensors. This concept was only briefly touched upon in this work.

Appendix A

ASD ANALYSIS

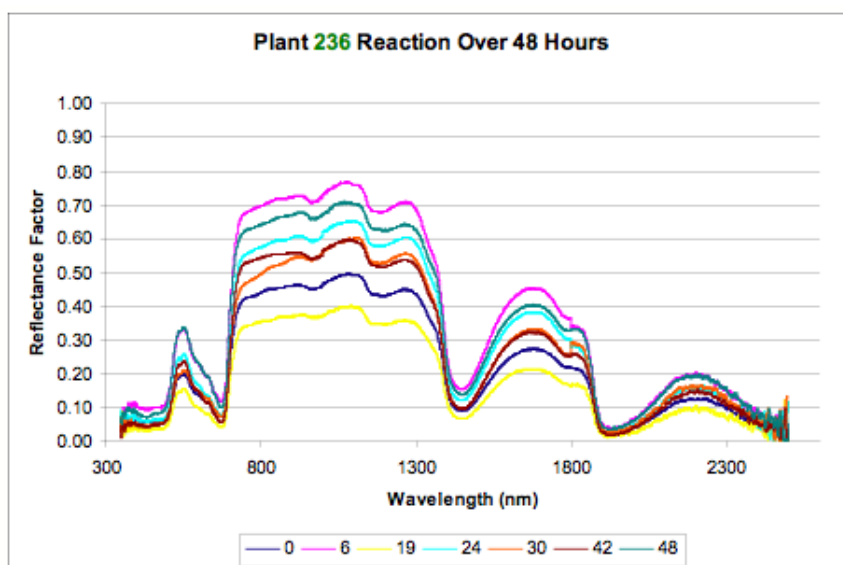


Figure A.1: ASD spectra of plant 236

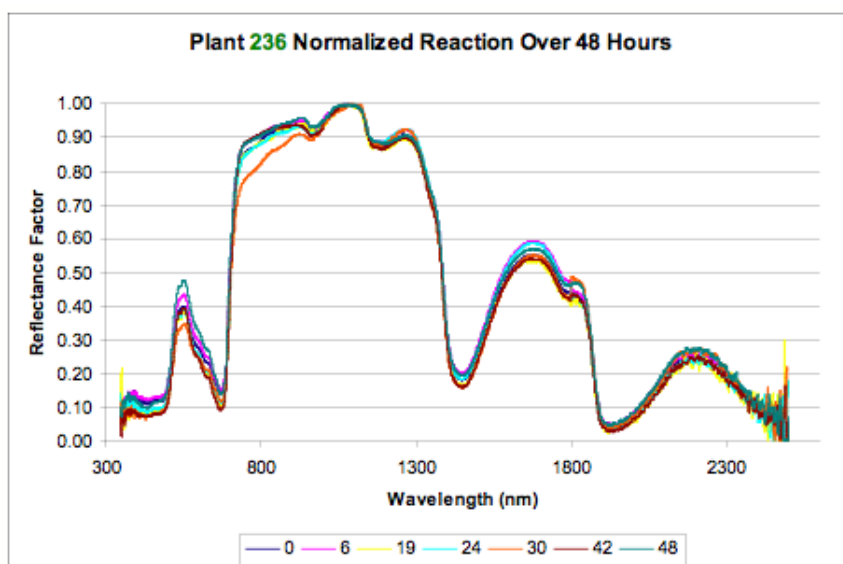


Figure A.2: ASD peak normalized spectra of plant 236

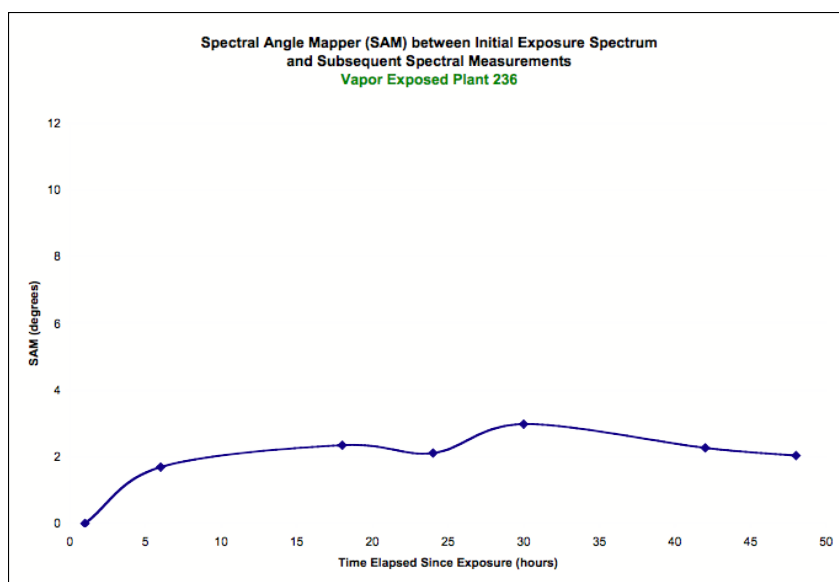


Figure A.3: Spectral Angle Mapper of ASD spectra of plant 236

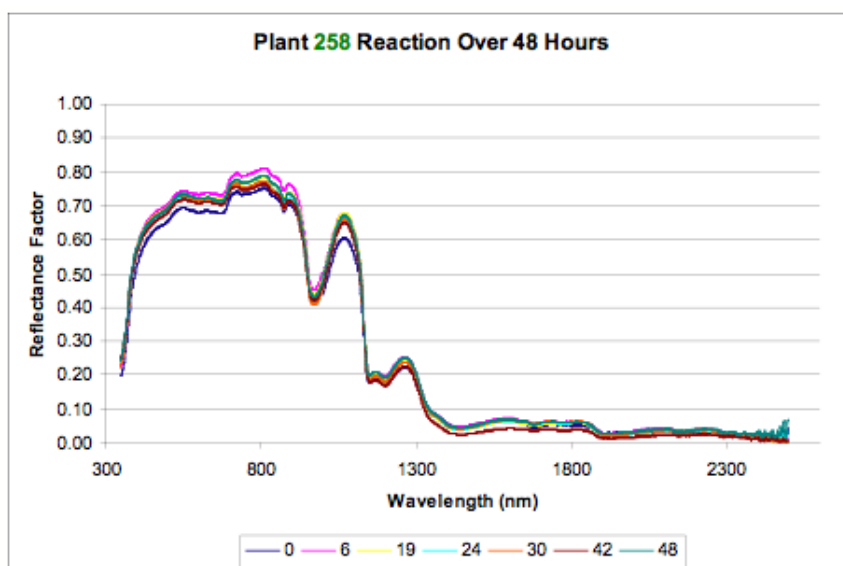


Figure A.4: ASD spectra of plant 258

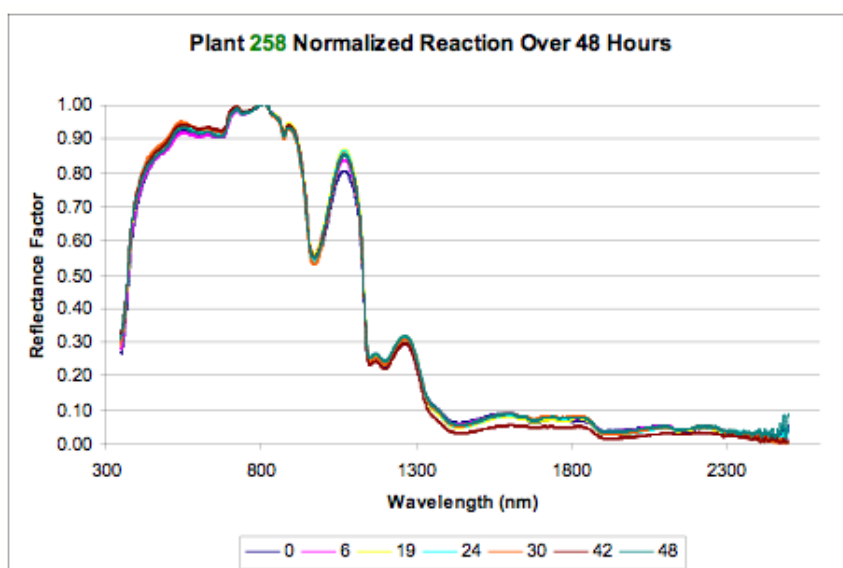


Figure A.5: ASD peak normalized spectra of plant 258

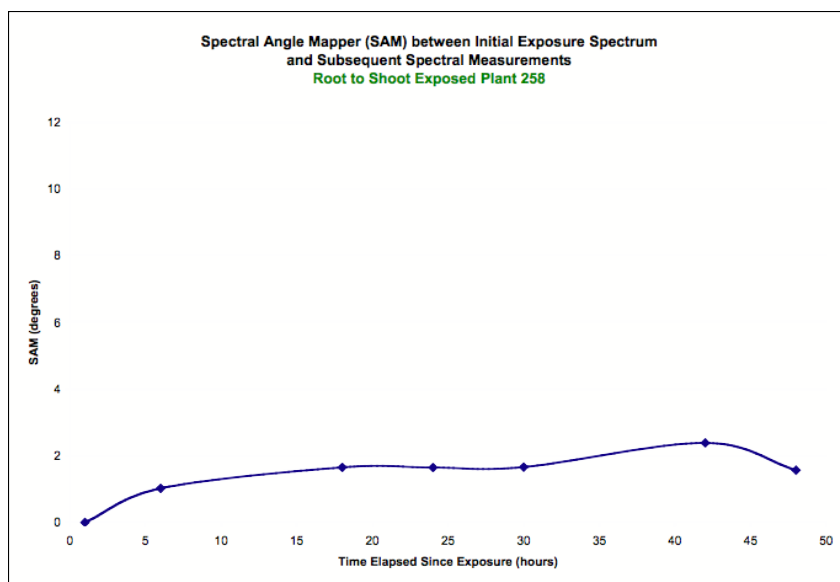


Figure A.6: Spectral Angle Mapper of ASD spectra of plant 258

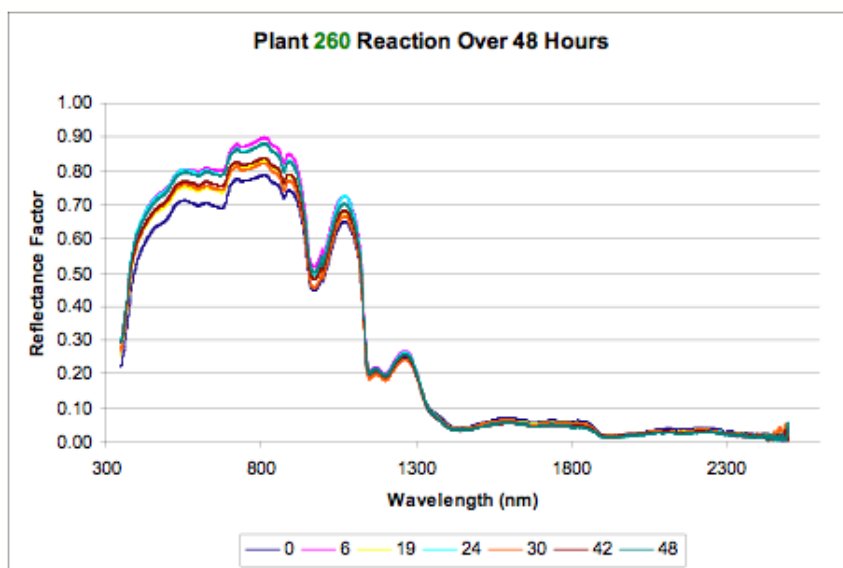


Figure A.7: ASD spectra of plant 260

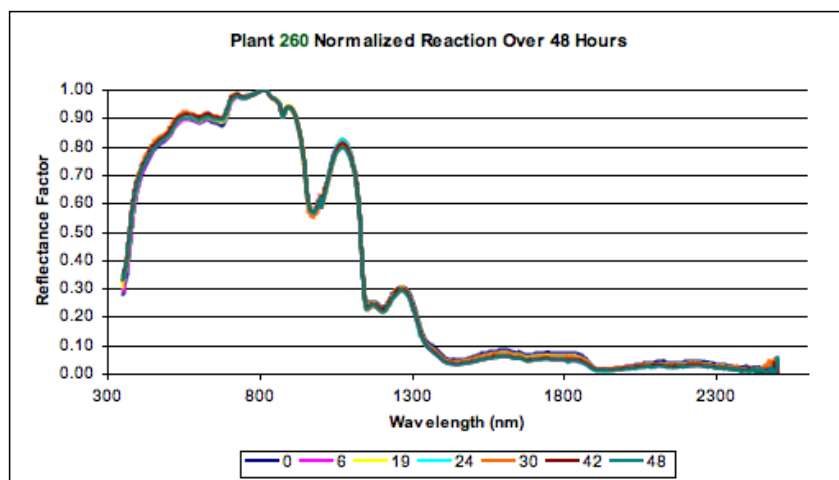


Figure A.8: ASD peak normalized spectra of plant 260

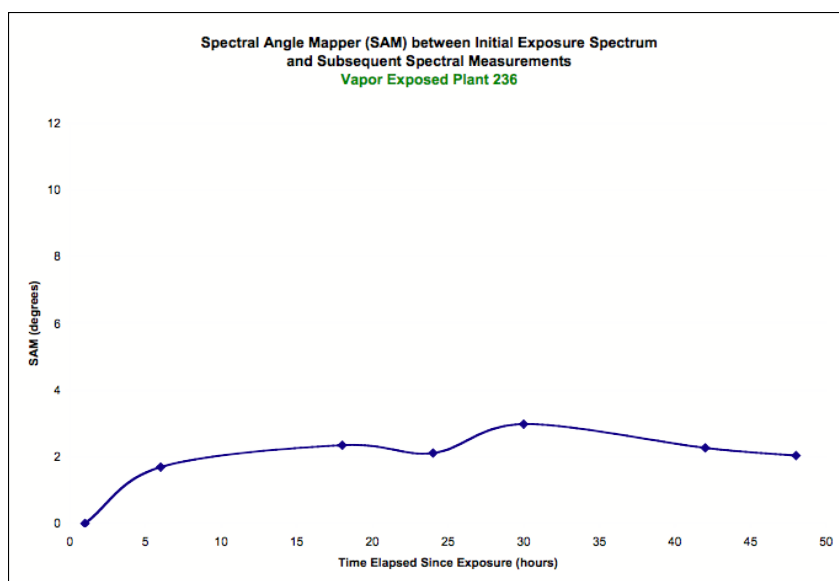


Figure A.9: Spectral Angle Mapper of ASD spectra of plant 260

Appendix B

IDL PROGRAMS

```
;Danielle Simmons
;Created: August 10, 2009

pro create_trade_study_images
side = 'left' ;left or right image
xy = 512
region = 'Full' ; full, BAOfull, BAOVIS, BAONIR
numbands = 251

;load in image to add noise and change bw on
filename = DIALOG_PICKFILE( )
pure_image = READ_BINARY(filename, DATA_TYPE=5 , $
DATA_DIMS=[xy, xy, numbands] )
print, 'done loading'

;select spectrum for SAM
specfile = dialog_pickfile()
specStruc = READ_ASCII(specfile, TEMPLATE=ASCII_TEMPLATE(specfile))
```

```

spec = specStruc.(1)

; ~~~~~
bands = indgen(251)
;bands = [46, 47, 48, 51, 54, 55, 56, 57, 58, 59, 60, 61, 96, 135,$
203, 205, 210, 248, 250] -1 ;BA0
;bands = [46, 47, 48, 51, 54, 55, 56, 57, 58, 59, 60, 61, 96] -1
;bands = [135, 203, 205, 210, 248, 250] -1

pure_image2 = TEMPORARY(pure_image[*,*,bands])
spec2 = TEMPORARY(spec[bands])
print, spec2

sizeim = size(bands)
numbands = sizeim[1]
noisy_image = add_noise(pure_image2, 50d, numBands)
OPENW, 2, '/Volumes/BIO-SENSORS/DIRSIG_SCENES/' + side + '_' + $
      string(xy, Format='(I0)') + '_' + region + '_5bw_50snr.img'
WRITEU, 2, noisy_image
CLOSE, 2
sam_image = SAM(noisy_image, spec2)
OPENW, 2, '/Volumes/BIO-SENSORS/DIRSIG_SCENES/' + side + '_' + $
      string(xy, Format='(I0)') + '_' + region + '_5bw_50snr_SAM.img'
WRITEU, 2, sam_image
CLOSE, 2
print, sam_image[0:2,0:2]

```

```

tvsc1, SAMimage

noisy_image = add_noise(pure_image2, 250d, numBands)
OPENW, 2, '/Volumes/BIO-SENSORS/DIRSIG_SCENES/' + side + '_' + $
        string(xy, Format='(I0)') + '_' + region + '_5bw_250snr.img'
WRITEU, 2, noisy_image
CLOSE, 2
sam_image = SAM(noisy_image, spec2)
OPENW, 2, '/Volumes/BIO-SENSORS/DIRSIG_SCENES/' + side + '_' + $
        string(xy, Format='(I0)') + '_' + region + '_5bw_250snr_SAM.img'
WRITEU, 2, sam_image
CLOSE, 2
print, sam_image[0:2,0:2]

noisy_image = add_noise(pure_image2, 500d, numBands)
OPENW, 2, '/Volumes/BIO-SENSORS/DIRSIG_SCENES/' + side + '_' + $
        string(xy, Format='(I0)') + '_' + region + '_5bw_500snr.img'
WRITEU, 2, noisy_image
CLOSE, 2
sam_image = SAM(noisy_image, spec2)
OPENW, 2, '/Volumes/BIO-SENSORS/DIRSIG_SCENES/' + side + '_' + $
        string(xy, Format='(I0)') + '_' + region + '_5bw_500snr_SAM.img'
WRITEU, 2, sam_image
CLOSE, 2
print, sam_image[0:2,0:2]

```

```

print, 'done with 5bw'

;-----

bw = 3 ; 10nm wide

bands = indgen(251)
;bands = [46, 47, 48, 50, 51, 52, 53, 54, 55, 56, 57, 58, 59,$
;         60, 61, 95, 96, 97, 134, 135, 136, 203, 204, 205, $
;         209, 210, 211, 248, 249, 250] -1
;bands = [46, 47, 48, 50, 51, 52, 53, 54, 55, 56, 57, 58, 59, $
;         60, 61, 95, 96, 97] -1
;bands = [134, 135, 136, 203, 204, 205, 209, 210, 211, 248,$
;         249, 250] -1

pure_image2 = TEMPORARY(pure_image[:,*,bands])
sizeim = size(bands)
numbands = sizeim[1]

bw_image = band_width(pure_image2, bw, numbands, xy)

spec2 = TEMPORARY(spec[bands])
spec2 = band_width(spec2, bw, numbands, 1)
spec2 = REFORM(TEMPORARY(spec2))

```

```
print, spec2

dimen = size(bw_image)
numBands2 = dimen[3]

noisy_image = add_noise(bw_image, 50d, numBands2)
OPENW, 2, '/Volumes/BIO-SENSORS/DIRSIG_SCENES/' + side + '_' + $
        string(xy, Format='(I0)') + '_' + region + '_10bw_50snr.img'
WRITEU, 2, noisy_image
CLOSE, 2

sam_image = SAM(noisy_image, spec2)
OPENW, 2, '/Volumes/BIO-SENSORS/DIRSIG_SCENES/' + side + '_' + $
        string(xy, Format='(I0)') + '_' + region + '_10bw_50snr_SAM.img'
WRITEU, 2, sam_image
CLOSE, 2

print, sam_image[0:2,0:2]

noisy_image = add_noise(bw_image, 250d, numBands2)
OPENW, 2, '/Volumes/BIO-SENSORS/DIRSIG_SCENES/' + side + '_' + $
        string(xy, Format='(I0)') + '_' + region + '_10bw_250snr.img'
WRITEU, 2, noisy_image
CLOSE, 2

sam_image = SAM(noisy_image, spec2)
OPENW, 2, '/Volumes/BIO-SENSORS/DIRSIG_SCENES/' + side + '_' + $
        string(xy, Format='(I0)') + '_' + region + '_10bw_250snr_SAM.img'
WRITEU, 2, sam_image
```

```

CLOSE, 2
print, sam_image[0:2,0:2]

noisy_image = add_noise(bw_image, 500d, numBands2)
OPENW, 2, '/Volumes/BIO-SENSORS/DIRSIG_SCENES/' + side + '_' + $
          string(xy, Format='(I0)') + '_' + region + '_10bw_500snr.img'
WRITEU, 2, noisy_image
CLOSE, 2
sam_image = SAM(noisy_image, spec2)
OPENW, 2, '/Volumes/BIO-SENSORS/DIRSIG_SCENES/' + side + '_' + $
          string(xy, Format='(I0)') + '_' + region + '_10bw_500snr_SAM.img'
WRITEU, 2, sam_image
CLOSE, 2
print, sam_image[0:2,0:2]

print, 'done with 10bw'

;-----
bw = 9 ; 40nm wide

bands = indgen(251)
;bands = [46, 47, 48, 49, 50, 51, 52, 53,
54, 55, 56, 57, 58, 59, 60, 61, 62, 63,$
;          92, 93, 94, 95, 96, 97, 98, 99, 100,
131, 132, 133, 134, 135, 136, 137,$

```



```

;          138, 139, 202, 203, 204, 205, 206,
207, 208, 209, 210, 243, 244, 245, $
;          246, 247, 248, 249, 250, 251] -1
;bands = [46, 47, 48, 49, 50, 51, 52, 53, 54,
55, 56, 57, 58, 59, 60, 61, 62, 63,$
;          92, 93, 94, 95, 96, 97, 98, 99, 100] -1
;bands = [131, 132, 133, 134, 135, 136, 137,
138, 139, 202, 203, 204, 205, 206, $
;          207, 208, 209, 210, 243, 244, 245, 246,
247, 248, 249, 250, 251] -1
pure_image2 = TEMPORARY(pure_image[:,*,bands])
sizeim = size(bands)
numbands = sizeim[1]

bw_image = band_width(pure_image2, bw, numbands, xy)

spec2 = TEMPORARY(spec[bands])
spec2 = band_width(spec2, bw, numbands, 1)
spec2 = REFORM(TEMPORARY(spec2))

print, spec2

dimen = size(bw_image)
numBands2 = dimen[3]

noisy_image = add_noise(bw_image, 50d, numBands2)
OPENW, 2, '/Volumes/BIO-SENSORS/DIRSIG_SCENES/' + side + '_' + $

```

```

        string(xy, Format='(I0)') + '_' + region + $
        '_40bw_50snr.img'
WRITEU, 2, noisy_image
CLOSE, 2
sam_image = SAM(noisy_image, spec2)
OPENW, 2, '/Volumes/BIO-SENSORS/DIRSIG_SCENES/' + side + '_' + $
        string(xy, Format='(I0)') + '_' + region + $
        '_40bw_50snr_SAM.img'
WRITEU, 2, sam_image
CLOSE, 2
print, sam_image[0:2,0:2]

```

```

noisy_image = add_noise(bw_image, 250d, numBands2)
OPENW, 2, '/Volumes/BIO-SENSORS/DIRSIG_SCENES/' + side + '_' + $
        string(xy, Format='(I0)') + '_' + region + $
        '_40bw_250snr.img'
WRITEU, 2, noisy_image
CLOSE, 2
sam_image = SAM(noisy_image, spec2)
OPENW, 2, '/Volumes/BIO-SENSORS/DIRSIG_SCENES/' + side + '_' + $
        string(xy, Format='(I0)') + '_' + region + $
        '_40bw_250snr_SAM.img'
WRITEU, 2, sam_image
CLOSE, 2
print, sam_image[0:2,0:2]

```

```

noisey_image = add_noise(bw_image, 500d, numBands2)
OPENW, 2, '/Volumes/BIO-SENSORS/DIRSIG_SCENES/' + side + '_' + $
        string(xy, Format='(I0)') + '_' + region + $
        '_40bw_500snr.img'
WRITEU, 2, noisey_image
CLOSE, 2
sam_image = SAM(noisey_image, spec2)
OPENW, 2, '/Volumes/BIO-SENSORS/DIRSIG_SCENES/' + side + '_' + $
        string(xy, Format='(I0)') + '_' + region + $
        '_40bw_500snr_SAM.img'
WRITEU, 2, sam_image
CLOSE, 2
print, sam_image[0:2,0:2]

print, 'done with 40bw'

;-----
bw = 33 ; 160nm wide

bands = indgen(251)
;bands = [3,4,5,6,7,8,9,10,11,12,13,14,15,16,17,18,19,20,21,22,23, $

```

```

;      24,25,26,27,28,29,30,31,32,33,34,35,36,37,38,39,40,41,42,$
;      43,44,45,46,47,48,49,50,51,52,53,54,55,56,57,58,59,60,61,$
;      62,63,64,65,66,67,68,69,70,71,72,73,74,75,76,77,78,79,80,$
;      81,82,83,84,85,86,87,88,89,90,91,92,93,94,95,96,97,98,99,$
;      100,101,116,117,118,119,120,121,122,123,124,125,126,127,$
;      128,129,130,131,132,133,134,135,136,137,138,139,140,141,$
;      142,143,144,145,146,147,148,186,187,188,189,190,191,192,$
;      193,194,195,196,197,198,199,200,201,202,203,204,205,206,$
;      207,208,209,210,211,212,213,214,215,216,217,218,219,220,$
;      221,222,223,224,225,226,227,228,229,230,231,232,233,234,$
;      235,236,237,238,239,240,241,242,243,244,245,246,247,248,$
;      249,250,251]-1
;bands = [3,4,5,6,7,8,9,10,11,12,13,14,15,16,17,18,19,20,21,22,23, $
;      24,25,26,27,28,29,30,31,32,33,34,35,36,37,38,39,40,41,42,$
;      43,44,45,46,47,48,49,50,51,52,53,54,55,56,57,58,59,60,61,$
;      62,63,64,65,66,67,68,69,70,71,72,73,74,75,76,77,78,79,80,$
;      81,82,83,84,85,86,87,88,89,90,91,92,93,94,95,96,97,98,99,$
;      100,101]-1
;bands = [116,117,118,119,120,121,122,123,124,125,126,127,$
;      128,129,130,131,132,133,134,135,136,137,138,139,140,141,$
;      142,143,144,145,146,147,148,186,187,188,189,190,191,192,$
;      193,194,195,196,197,198,199,200,201,202,203,204,205,206,$
;      207,208,209,210,211,212,213,214,215,216,217,218,219,220,$
;      221,222,223,224,225,226,227,228,229,230,231,232,233,234,$
;      235,236,237,238,239,240,241,242,243,244,245,246,247,248,$
;      249,250,251]-1
pure_image2 = TEMPORARY(pure_image[*,* ,bands])

```

```
sizeim = size(bands)
numbands = sizeim[1]

bw_image = band_width(pure_image2, bw, numbands, xy)

spec2 = TEMPORARY(spec[bands])
spec2 = band_width(spec2, bw, numbands, 1)
spec2 = REFORM(TEMPORARY(spec2))

dimen = size(bw_image)
numBands2 = dimen[3]

print, spec2

noisy_image = add_noise(bw_image, 50d, numBands2)
OPENW, 2, '/Volumes/BIO-SENSORS/DIRSIG_SCENES/' + side + '_' + $
    string(xy, Format='(I0)') + '_' + region + $
    '_160bw_50snr.img'
WRITEU, 2, noisy_image
CLOSE, 2

sam_image = SAM(noisy_image, spec2)
OPENW, 2, '/Volumes/BIO-SENSORS/DIRSIG_SCENES/' + side + '_' + $
    string(xy, Format='(I0)') + '_' + region + $
    '_160bw_50snr_SAM.img'
WRITEU, 2, sam_image
CLOSE, 2
print, sam_image[0:2,0:2]
```

```
noisy_image = add_noise(bw_image, 250d, numBands2)
OPENW, 2, '/Volumes/BIO-SENSORS/DIRSIG_SCENES/' + side + '_' + $
        string(xy, Format='(I0)') + '_' + region + $
        '_160bw_250snr.img'
WRITEU, 2, noisy_image
CLOSE, 2
sam_image = SAM(noisy_image, spec2)
OPENW, 2, '/Volumes/BIO-SENSORS/DIRSIG_SCENES/' + side + '_' + $
        string(xy, Format='(I0)') + '_' + region + $
        '_160bw_250snr_SAM.img'
WRITEU, 2, sam_image
CLOSE, 2
print, sam_image[0:2,0:2]
```

```
noisy_image = add_noise(bw_image, 500d, numBands2)
OPENW, 2, '/Volumes/BIO-SENSORS/DIRSIG_SCENES/' + side + '_' + $
        string(xy, Format='(I0)') + '_' + region + $
        '_160bw_500snr.img'
WRITEU, 2, noisy_image
CLOSE, 2
sam_image = SAM(noisy_image, spec2)
OPENW, 2, '/Volumes/BIO-SENSORS/DIRSIG_SCENES/' + side + '_' + $
        string(xy, Format='(I0)') + '_' + region + $
        '_160bw_500snr_SAM.img'
```

```

WRITEU, 2, sam_image
CLOSE, 2
print, sam_image[0:2,0:2]

print, 'done with 160bw'
print, 'fini'

END

;*****

FUNCTION band_width, image, bw, numBands, xy
;THIS FUNCTION SELECTS BANDS AND BANDWIDTH (bw)

dimen = size(image)

IF dimen[0] EQ 1 THEN BEGIN
    ;apply a rect to image in z direction
    smoothed_image = SMOOTH(image, bw)
    smoothed_image = REFORM(smoothed_image, [1, 1, dimen[3]])
ENDIF ELSE BEGIN
    ;apply a rect to image in z direction
    smoothed_image = SMOOTH(image, [1,1,bw])
ENDELSE

    ; Define how many bands will be in the new image and

```

```

; make an array to hold new image
newnumbands = FLOOR( numbands / DOUBLE(bw) )
bw_image = DBLARR(xy,xy,newnumbands)
start = FLOOR( DOUBLE(bw) / 2 )
smoothed_image = TEMPORARY(smoothed_image[*,*,start:numbands-1])

FOR i = 0, numbands-bw, bw DO BEGIN
    ;assign smoothed band to bw_image
    bw_image[*,*,i/bw] = smoothed_image[*,*,i]
ENDFOR

RETURN, bw_image

END

;*****

FUNCTION add_noise, image, snr, numBands
;THIS FUNCTION CALCULATES NOISE BASED ON IMAGE STATS.

;1. a SNR value is assigned.
;2. the average signal (or average of all the bands) is computed
;3. the standard deviation of the noise is determined as average
;   signal divided by NSR value
;4. the standard dev is multiplied by a normally distributed
;   random number generator
;

```



```

;compute average signal
avgSignal = DBLARR(1,1,numBands)
FOR k = 0, numbands-1, 1 DO BEGIN
    avgSignal[k] = MEAN(image[*,*,k])
ENDFOR

;Define SNR value and compute noise standard deviation
sig = avgSignal / snr

;Create noise image for each band
noise = DBLARR(512,512,numbands)
FOR k = 0, numbands-1, 1 DO BEGIN
    noise[*,*,k] = sig[k] * randomn(12, 512, 512, /DOUBLE, /NORMAL)
ENDFOR

;add each noise image for each band to original image

noisy_image = image + noise

RETURN, noisy_image

END

;*****

function SAM, image, spectra
;reform spectra in upper prog

```

```
dimen = size(image)

SAMimage = dblarr(dimen[1],dimen[2])

FOR x = 0, dimen[1]-1 DO BEGIN
  FOR y = 0, dimen[2]-1 DO BEGIN
    temp = reform( image(x,y,*), 1, dimen[3] )
    SAMimage[x,y] = (temp # spectra) / $
                     (sqrt(temp # reform(image(x,y,*)) ) &
                      * sqrt(transpose(spectra) # spectra))
    maxSI = max(SAMimage)
    IF maxSI GT 1D THEN SAMimage[&
WHERE(SAMimage GT 1D)] = 1D
    SAMimage = acox(SAMimage)
  END
END

RETURN, SAMimage

END
```

Appendix C

MATLAB PROGRAMS

```
% Danielle Simmons
% This program is a script that runs the ROC.m on every file in a
% directory. It saves the ROC curves and the area under the ROC
% curves out to file.

clear

[SAMfiles, SAMpaths] = uigetfile('*.img','...
Select a group of SAM images to analyze', 'MultiSelect', 'on');
numfiles = numel(SAMfiles);
[TruthFile, TruthPath] = uigetfile('*.img','Select DIRSIG truth...
data');
nfpa = 512;

SAMareaArr = zeros(numfiles,1);
```

```

for i=1:numfiles
    SAM = multibandread([SAMpaths SAMfiles{i}],[nfpa nfpa, 1],...
        'double',0,'bsq','native',{'Band','Direct',[1]});
    [SAMpfa, SAMpd] = ROC(TruthFile, TruthPath, SAM, nfpa);
    % Find the area under the ROC curve
    SAMareaArr(i) = max( cumtrapz(SAMpfa, SAMpd) )

    % plot ROC curve and save
    figure(1)
    plot(SAMpfa,SAMpd,'-r')
    title(SAMfiles(i),'Interpreter','none', 'fonts', 18 )
    xlabel( 'False Alarm Rate', 'fonts', 16 )
    ylabel( 'Detection Rate' , 'fonts', 16 )
    figuretitle = strrep(SAMfiles{i}, '.img', '_plot');
    saveas(1, figuretitle, 'png')

end

areas{1} = SAMfiles;
areas{2} = SAMareaArr;

save right_512_AUC.txt SAMareaArr -ASCII

```

```

function [ CEMPFA, CEMPD] = ROC(TruthFile, TruthPath, CEM, nfpa)
% This program is to be used after the ResizeHSI program
% produces a fusion score for each pixel
%
if nargin == 0
    close all;
    clear all;
    clc;
    [SAMFile, SAMPath] = uigetfile('*.img',...
    'Select SAM image to analyze');
    [TruthFile, TruthPath] = uigetfile('*.img',...
    'Select DIRSIG truth data');
    nfpa = 512; %dimension
    CEM = multibandread([SAMPath SAMFile],[nfpa nfpa, 1],...
    'double',0,'bsq','native',{'Band','Direct',[1]});
end

% Load pixel material truth map, ID which pixels match the
% target material 9210 (degreened biosensor)
TruthMat = multibandread([TruthPath TruthFile],[nfpa nfpa 1],...
'double',0,'bsq','native',{'Band','Direct',[1]}); %check
Target = TruthMat==9210;

% Determine Fusion and CEM scores of Target pixels
TargetCEM = CEM(Target);

```

```
% Sort the target scores from greatest to least

TargetCEM = sort(TargetCEM,'descend');
numtargets = length(TargetCEM);

% determine number of pixels with actual data in them
% (potential false alarms)
SpectralPixels = nfpa^2;

%% This section is for integrating to PFA = 0.01
cutoff = 0.01;

% Calculate the ROC curve
CEMPFA_Full = zeros(numtargets,1);
CEMPD_Full = zeros(numtargets,1);

for i = 1:numtargets
    CEMCount = find(CEM>=TargetCEM(i));
    CEMFA = length(CEMCount)-i;
    CEMPFA_Full(i) = CEMFA/SpectralPixels;
    CEMPD_Full(i) = i/numtargets;
end
```

```

% Check to determine whether targets were found before
% the PFA cutoff
ValidCEM = find(CEMPFA_Full <= cutoff);
TF_CEM = isempty(ValidCEM);

if TF_CEM == 0
    error_CEM = 0;
    % Determine whether all targets were found before cutoff
    if length(ValidCEM) == numtargets
        CEMPFA = CEMPFA_Full;
        CEMPD = CEMPD_Full;
    else
        % Interpolate to find PD at PFA = cutoff
        n_CEM = length(ValidCEM);
        b_CEM = CEMPD_Full(n_CEM);
        m_CEM = (CEMPD_Full(n_CEM+1)-CEMPD_Full(n_CEM))/...
            (CEMPFA_Full(n_CEM+1)...
            -CEMPFA_Full(n_CEM));
        x_CEM = cutoff-CEMPFA_Full(n_CEM);
        y_CEM = m_CEM*x_CEM+b_CEM;

    % Capture ROC curve values to the left of
    % PFA = cutoff, include interpolated point
        CEMPFA = zeros(n_CEM+1,1);
        CEMPD = zeros(n_CEM+1,1);

```

```

        CEMPFA(1:n_CEM) = CEMPFA_Full(ValidCEM);
        CEMPD(1:n_CEM) = CEMPD_Full(ValidCEM);
        CEMPFA(n_CEM+1) = cutoff;
        CEMPD(n_CEM+1) = y_CEM;
    end

    % Find the area under the CEM curve
    CEMArea = cumtrapz(CEMPFA,CEMPD);

else
    error_CEM = 1;
    CEMPFA = 0;
    CEMPD = 0;
end

%% make surface plots of ROC curve area

leftbig050 =
    [8.9940868e-01    8.8657645e-01    8.9728889e-01    9.0129100e-01;...
     9.0891097e-01    9.0465560e-01    9.0636268e-01    9.0887292e-01;...
     9.0129038e-01    8.8799983e-01    8.9842758e-01    9.0450941e-01;...
     8.9061664e-01    8.8724792e-01    8.8992762e-01    8.9073865e-01];

figure(1)

```



```

surf(leftbig050)
title('ROC AUC - Left 512x512 Pixels - SNR 50', 'fontsize', 14)
y ={'BAO-Full'; 'BAO-NIR'; 'BAO-VIS';'Full'};
y = char(y);
x = [5,10,40,160];
set(gca,'XTick',[1:4], 'XTickLabel', {x})
set(gca,'YTick',[1:4], 'YTickLabel', {y})
zlim([0 1.0]);
xlabel('Bandwidth (nm)', 'fontsize', 12);
ylabel('Spectral Region Subset', 'fontsize', 12);
zlabel('ROC AUC', 'fontsize', 12);
caxis([0 0.01])
colormap(jet)

leftbig250 =
[ 8.9261337e-01    8.8098334e-01    8.8974153e-01    8.9567154e-01;...
  9.1180823e-01    9.0830214e-01    9.0872902e-01    9.0994490e-01;...
  8.9814454e-01    8.8487798e-01    8.9198708e-01    9.0310046e-01;...
  8.8716630e-01    8.8473216e-01    8.8652951e-01    8.8722456e-01 ];

figure(2)
surf(leftbig250)
title('ROC AUC - Left 512x512 Pixels - SNR 250', 'fontsize', 14)
y ={'BAO-Full'; 'BAO-NIR'; 'BAO-VIS';'Full'};
y = char(y);

```

```

x = [5,10,40,160];
set(gca,'XTick',[1:4], 'XTickLabel', {x})
set(gca,'YTick',[1:4], 'YTickLabel', {y})
zlim([0 1.0]);
xlabel('Bandwidth (nm)', 'fontsize', 12);
ylabel('Spectral Region Subset', 'fontsize', 12);
zlabel('ROC AUC', 'fontsize', 12);
caxis([0 0.01])
colormap(jet)

leftbig500 =
    [8.9051314e-01    8.8056491e-01    8.8785657e-01    8.8467437e-01;...
      9.1244019e-01    9.0804763e-01    9.0789548e-01    9.0648176e-01;...
      8.9611555e-01    8.8471904e-01    8.8970029e-01    8.9286804e-01;...
      8.8683556e-01    8.8439885e-01    8.8620654e-01    8.8689013e-01 ];

figure(3)
surf(leftbig500)
title('ROC AUC - Left 512x512 Pixels - SNR 500', 'fontsize', 14)
y = {'BA0-Full'; 'BA0-NIR'; 'BA0-VIS'; 'Full'};
y = char(y);
x = [5,10,40,160];
set(gca,'XTick',[1:4], 'XTickLabel', {x})
set(gca,'YTick',[1:4], 'YTickLabel', {y})
zlim([0 1.0]);

```

```

xlabel('Bandwidth (nm)','fontsize',12);
ylabel('Spectral Region Subset','fontsize',12);
zlabel('ROC AUC', 'fontsize',12);
caxis([0 0.01])
colormap(jet)

leftmed050 =
[ 8.8895901e-01   8.6189673e-01   8.8732513e-01   8.8598108e-01;...
  8.8290985e-01   8.7228421e-01   8.7645480e-01   8.8633835e-01;...
  8.8806772e-01   8.7970563e-01   8.8785242e-01   8.8659525e-01;...
  8.8533459e-01   8.7752393e-01   8.8351480e-01   8.8520627e-01];

figure(4)
surf(leftmed050)
title('ROC AUC - Left 128x128 Pixels - SNR 50', 'fontsize', 14)
y ={'BAO-Full'; 'BAO-NIR'; 'BAO-VIS';'Full'};
y = char(y);
x = [5,10,40,160];
set(gca,'XTick',[1:4], 'XTickLabel', {x})
set(gca,'YTick',[1:4], 'YTickLabel', {y})
zlim([0 1.0]);
xlabel('Bandwidth (nm)','fontsize',12);
ylabel('Spectral Region Subset','fontsize',12);
zlabel('ROC AUC', 'fontsize',12);
caxis([0 0.01])

```

```

colormap(jet)

leftmed250 =
[ 8.9849078e-01    8.6576727e-01    8.9670648e-01    8.9684448e-01;...
  8.9837491e-01    8.9199255e-01    8.9692169e-01    8.9895895e-01;...
  8.9808453e-01    8.8168475e-01    8.9652728e-01    8.9763873e-01;...
  8.8732526e-01    8.7988184e-01    8.8601306e-01    8.8750281e-01 ];

figure(5)
surf(leftmed250)
title('ROC AUC - Left 128x128 Pixels - SNR 250', 'fontsize', 14)
y ={'BAO-Full'; 'BAO-NIR'; 'BAO-VIS'; 'Full'};
y = char(y);
x = [5,10,40,160];
set(gca,'XTick',[1:4], 'XTickLabel', {x})
set(gca,'YTick',[1:4], 'YTickLabel', {y})
zlim([0 1.0]);
xlabel('Bandwidth (nm)', 'fontsize', 12);
ylabel('Spectral Region Subset', 'fontsize', 12);
zlabel('ROC AUC', 'fontsize', 12);
caxis([0 0.01])
colormap(jet)

leftmed500 =

```

```

[9.0003497e-01    8.6598828e-01    8.9736090e-01    8.9882913e-01;...
 9.0348300e-01    8.9864087e-01    9.0236069e-01    9.0340607e-01;...
 8.9956165e-01    8.8163837e-01    8.9711230e-01    8.9996637e-01;...
 8.8742194e-01    8.7985840e-01    8.8611975e-01    8.8758911e-01];

figure(6)
surf(leftmed500)
title('ROC AUC - Left 128x128 Pixels - SNR 500', 'fontsize', 14)
y ={'BAO-Full'; 'BAO-NIR'; 'BAO-VIS';'Full'};
y = char(y);
x = [5,10,40,160];
set(gca,'XTick',[1:4], 'XTickLabel', {x})
set(gca,'YTick',[1:4], 'YTickLabel', {y})
zlim([0 1.0]);
xlabel('Bandwidth (nm)', 'fontsize', 12);
ylabel('Spectral Region Subset', 'fontsize', 12);
zlabel('ROC AUC', 'fontsize', 12);
caxis([0 0.01])
colormap(jet)

leftsm050 =
[8.3007125e-01    6.9281608e-01    5.7995434e-01    8.3207939e-01;...
 3.4002943e-01    3.3575182e-01    3.0496947e-01    3.7444295e-01;...
 8.2958984e-01    7.8118123e-01    8.1224554e-01    8.3085525e-01;...
```

```

7.3062005e-01    7.3496644e-01    7.2985668e-01    7.3062005e-01 ];

figure(7)
surf(leftsm050)
title('ROC AUC - Left 32x32 Pixels - SNR 50', 'fontsize', 14)
y ={'BAO-Full'; 'BAO-NIR'; 'BAO-VIS';'Full'};
y = char(y);
x = [5,10,40,160];
set(gca,'XTick',[1:4], 'XTickLabel', {x})
set(gca,'YTick',[1:4], 'YTickLabel', {y})
zlim([0 1.0]);
xlabel('Bandwidth (nm)', 'fontsize', 12);
ylabel('Spectral Region Subset', 'fontsize', 12);
zlabel('ROC AUC', 'fontsize', 12);
caxis([0 0.01])
colormap(jet)

leftsm250 =
[8.3474774e-01    6.9314618e-01    5.6532653e-01    8.3166676e-01;...
 3.2935602e-01    3.3651518e-01    3.2351728e-01    3.0522392e-01;...
 8.2921847e-01    7.7506052e-01    8.2388864e-01    8.3108907e-01;...
 7.3110833e-01    7.1789035e-01    7.2992545e-01    7.2936152e-01 ];

figure(8)

```

```

surf(leftsm250)
title('ROC AUC - Left 32x32 Pixels - SNR 250', 'fontsize', 14)
y ={'BAO-Full'; 'BAO-NIR'; 'BAO-VIS';'Full'};
y = char(y);
x = [5,10,40,160];
set(gca,'XTick',[1:4], 'XTickLabel', {x})
set(gca,'YTick',[1:4], 'YTickLabel', {y})
zlim([0 1.0]);
xlabel('Bandwidth (nm)', 'fontsize', 12);
ylabel('Spectral Region Subset', 'fontsize', 12);
zlabel('ROC AUC', 'fontsize', 12);
caxis([0 0.01])
colormap(jet)

leftsm500 =
[8.3495406e-01  6.9045720e-01  5.5740399e-01  8.3177679e-01;...
 3.2078015e-01  3.3720978e-01  3.1816681e-01  3.1119333e-01;...
 8.2928725e-01  7.7136059e-01  6.4251623e-01  8.3100655e-01;...
 7.3106707e-01  7.1685189e-01  7.3090889e-01  7.2937528e-01 ];

figure(9)
surf(leftsm500)
title('ROC AUC - Left 32x32 Pixels - SNR 500', 'fontsize', 14)
y ={'BAO-Full'; 'BAO-NIR'; 'BAO-VIS';'Full'};

```

```

y = char(y);
x = [5,10,40,160];
set(gca,'XTick',[1:4], 'XTickLabel', {x})
set(gca,'YTick',[1:4], 'YTickLabel', {y})
zlim([0 1.0]);
xlabel('Bandwidth (nm)', 'fontsize', 12);
ylabel('Spectral Region Subset', 'fontsize', 12);
zlabel('ROC AUC', 'fontsize', 12);
caxis([0 0.01])
colormap(jet)
%%

%+++++RIGHT+++++

rightbig050 =
[ 9.0321552e-01    8.8399724e-01    8.9795641e-01    9.0961001e-01;...
  9.1726732e-01    9.1249288e-01    9.1548714e-01    9.1731235e-01;...
  9.1135684e-01    8.8205694e-01    9.0380947e-01    9.1878427e-01;...
  8.8450464e-01    8.8121204e-01    8.8401474e-01    8.8457090e-01 ];

figure(10)
surf(rightbig050)
title('ROC AUC - Right 512x512 Pixels - SNR 50', 'fontsize', 14)
y = {'BAO-Full'; 'BAO-NIR'; 'BAO-VIS'; 'Full'};
y = char(y);

```



```

x = [5,10,40,160];
set(gca,'XTick',[1:4], 'XTickLabel', {x})
set(gca,'YTick',[1:4], 'YTickLabel', {y})
zlim([0 1.0]);
xlabel('Bandwidth (nm)', 'fontsize', 12);
ylabel('Spectral Region Subset', 'fontsize', 12);
zlabel('ROC AUC', 'fontsize', 12);
caxis([0 0.01])
colormap(jet)

rightbig250 =
[ 8.9555325e-01   8.8117051e-01   8.8952876e-01   9.0091530e-01;...
  9.2782445e-01   9.2487759e-01   9.2390784e-01   9.2709210e-01;...
  9.0884862e-01   8.8057379e-01   8.9822477e-01   9.2207956e-01;...
  8.8343783e-01   8.8052016e-01   8.8319424e-01   8.8348381e-01  ];

figure(11)
surf(rightbig250)
title('ROC AUC - Right 512x512 Pixels - SNR 250', 'fontsize', 14)
y = {'BAO-Full'; 'BAO-NIR'; 'BAO-VIS'; 'Full'};
y = char(y);
x = [5,10,40,160];
set(gca,'XTick',[1:4], 'XTickLabel', {x})

```

```

set(gca,'YTick',[1:4], 'YTickLabel', {y})
zlim([0 1.0]);
xlabel('Bandwidth (nm)', 'fontsize', 12);
ylabel('Spectral Region Subset', 'fontsize', 12);
zlabel('ROC AUC', 'fontsize', 12);
caxis([0 0.01])
colormap(jet)

rightbig500 =
    [8.9302858e-01    8.8120989e-01    8.8981756e-01    8.9657814e-01;...
     9.3061467e-01    9.2533038e-01    9.2303763e-01    9.2944251e-01;...
     9.0760541e-01    8.8036063e-01    8.9475678e-01    9.2405434e-01;...
     8.8461366e-01    8.8068234e-01    8.8429570e-01    8.8466745e-01    ];

figure(12)
surf(rightbig500)
title('ROC AUC - Right 512x512 Pixels - SNR 500', 'fontsize', 14)
y = {'BAO-Full'; 'BAO-NIR'; 'BAO-VIS'; 'Full'};
y = char(y);
x = [5,10,40,160];
set(gca,'XTick',[1:4], 'XTickLabel', {x})
set(gca,'YTick',[1:4], 'YTickLabel', {y})
zlim([0 1.0]);
xlabel('Bandwidth (nm)', 'fontsize', 12);

```

```

ylabel('Spectral Region Subset','fontsize',12);
xlabel('ROC AUC', 'fontsize',12);
caxis([0 0.01])
colormap(jet)

rightmed050 =
[ 9.0503403e-01    8.9545662e-01    9.0524628e-01    9.0142361e-01;...
  8.7129479e-01    8.7441917e-01    8.7116164e-01    8.7712726e-01;...
  9.0944625e-01    9.1570298e-01    9.2089171e-01    8.9970392e-01;...
  9.0559393e-01    8.9828130e-01    9.0202176e-01    9.0559917e-01 ];

figure(13)
surf(rightmed050)
title('ROC AUC - Right 128x128 Pixels - SNR 50', 'fontsize', 14)
y ={'BAO-Full'; 'BAO-NIR'; 'BAO-VIS';'Full'};
y = char(y);
x = [5,10,40,160];
set(gca,'XTick',[1:4], 'XTickLabel', {x})
set(gca,'YTick',[1:4], 'YTickLabel', {y})
zlim([0 1.0]);
xlabel('Bandwidth (nm)','fontsize',12);
ylabel('Spectral Region Subset','fontsize',12);
xlabel('ROC AUC', 'fontsize',12);
caxis([0 0.01])

```

```

colormap(jet)

rightmed250 =
    [8.9317004e-01    9.0689685e-01    9.3531145e-01    8.8594236e-01;...
     9.1324463e-01    9.1014342e-01    9.1177094e-01    9.1578955e-01;...
     8.9600195e-01    9.0537670e-01    9.4684075e-01    8.9723623e-01;...
     8.5835297e-01    9.1097151e-01    8.6489295e-01    8.5413507e-01 ];

figure(14)
surf(rightmed250)
title('ROC AUC - Right 128x128 Pixels - SNR 250', 'fontsize', 14)
y ={'BAO-Full'; 'BAO-NIR'; 'BAO-VIS'; 'Full'};
y = char(y);
x = [5,10,40,160];
set(gca,'XTick',[1:4], 'XTickLabel', {x})
set(gca,'YTick',[1:4], 'YTickLabel', {y})
zlim([0 1.0]);
xlabel('Bandwidth (nm)', 'fontsize', 12);
ylabel('Spectral Region Subset', 'fontsize', 12);
zlabel('ROC AUC', 'fontsize', 12);
caxis([0 0.01])
colormap(jet)

```

```
rightmed500 =
[ 8.8362614e-01    8.9213655e-01    9.3570370e-01    8.9334231e-01;...
  9.2832480e-01    9.2991844e-01    9.2892344e-01    9.3220763e-01;...
  8.7640119e-01    9.0417941e-01    9.3453469e-01    8.9891345e-01;...
  8.5133617e-01    8.9722402e-01    8.6497392e-01    8.4744362e-01    ];
```

```
figure(15)
surf(rightmed500)
title('ROC AUC - Right 128x128 Pixels - SNR 500', 'fontsize', 14)
y ={'BA0-Full'; 'BA0-NIR'; 'BA0-VIS'; 'Full'};
y = char(y);
x = [5,10,40,160];
set(gca,'XTick',[1:4], 'XTickLabel', {x})
set(gca,'YTick',[1:4], 'YTickLabel', {y})
zlim([0 1.0]);
xlabel('Bandwidth (nm)', 'fontsize', 12);
ylabel('Spectral Region Subset', 'fontsize', 12);
zlabel('ROC AUC', 'fontsize', 12);
caxis([0 0.01])
colormap(jet)
```

```
rightsm050 =
[ 1.6973199e-01    7.5054253e-01    2.4370660e-01    2.2631836e-01;...
  3.3981662e-01    3.1700304e-01    2.9966905e-01    3.4670681e-01;...
```

```

2.2102865e-01    2.4218750e-01    1.4097765e-01    2.3765734e-01;...
4.8168945e-01    4.3229167e-01    4.7984484e-01    4.8253038e-01];

figure(16)
surf(rightsm050)
title('ROC AUC - Right 32x32 Pixels - SNR 50', 'fontsize', 14)
y ={'BA0-Full'; 'BA0-NIR'; 'BA0-VIS'; 'Full'};
y = char(y);
x = [5,10,40,160];
set(gca,'XTick',[1:4], 'XTickLabel', {x})
set(gca,'YTick',[1:4], 'YTickLabel', {y})
zlim([0 1.0]);
xlabel('Bandwidth (nm)', 'fontsize', 12);
ylabel('Spectral Region Subset', 'fontsize', 12);
zlabel('ROC AUC', 'fontsize', 12);
caxis([0 0.01])
colormap(jet)

rightsm250 =
[1.7797852e-01    7.5770399e-01    1.3262261e-01    2.4560547e-01;...
 3.0376519e-01    3.7122938e-01    3.0862088e-01    3.0541992e-01;...
 2.1489800e-01    2.4405924e-01    1.1642795e-01    2.5689019e-01;...
 4.9145508e-01    4.6126302e-01    4.8955621e-01    4.9161784e-01];

```

```

figure(17)
surf(rightsm250)
title('ROC AUC - Right 32x32 Pixels - SNR 250', 'fontsize', 14)
y ={'BAO-Full'; 'BAO-NIR'; 'BAO-VIS';'Full'};
y = char(y);
x = [5,10,40,160];
set(gca,'XTick',[1:4], 'XTickLabel', {x})
set(gca,'YTick',[1:4], 'YTickLabel', {y})
zlim([0 1.0]);
xlabel('Bandwidth (nm)', 'fontsize', 12);
ylabel('Spectral Region Subset', 'fontsize', 12);
zlabel('ROC AUC', 'fontsize', 12);
caxis([0 0.01])
colormap(jet)

rightsm500 =
    [1.8250868e-01    7.5868056e-01    1.2999132e-01    2.4997287e-01;...
     3.1190321e-01    3.7177192e-01    3.1575521e-01    3.1198459e-01;...
     2.1177843e-01    2.4126519e-01    1.0101997e-01    2.5935872e-01;...
     4.9145508e-01    4.6237522e-01    4.9134657e-01    4.9145508e-01];

figure(18)
surf(rightsm500)
title('ROC AUC - Right 32x32 Pixels - SNR 500', 'fontsize', 14)
y ={'BAO-Full'; 'BAO-NIR'; 'BAO-VIS';'Full'};

```

```

y = char(y);
x = [5,10,40,160];
set(gca,'XTick',[1:4], 'XTickLabel', {x})
set(gca,'YTick',[1:4], 'YTickLabel', {y})
zlim([0 1.0]);
xlabel('Bandwidth (nm)', 'fontsize', 12);
ylabel('Spectral Region Subset', 'fontsize', 12);
zlabel('ROC AUC', 'fontsize', 12);
caxis([0 0.01])
colormap(jet)

%%
clear

rightsm500 =
[8.8806772e-01    8.7970563e-01    8.8785242e-01    8.8659525e-01;...
    8.9808453e-01    8.8168475e-01    8.9652728e-01    8.9763873e-01;...
    8.9956165e-01    8.8163837e-01    8.9711230e-01    8.9996637e-01];

figure(18)
surf(rightsm500)
title('ROC AUC - SNR vs. BW of Left 128x128 BAOVIS', 'fontsize', 14)
x = {'5'; '10'; '40'; '60'};
x = char(x);
y = {'50'; '250'; '500'};

```



```
y = char(y);  
set(gca,'XTick',[1:4], 'XTickLabel', {x})  
set(gca,'YTick',[1:4], 'YTickLabel', {y})  
zlim([.8 1.0]);  
xlabel('Bandwidth (nm)','fontsize',12);  
ylabel('Spectral Region Subset','fontsize',12);  
zlabel('ROC AUC', 'fontsize',12);  
caxis([0 0.01])  
colormap(jet)
```

Bibliography

- [1] Mauricio S. Antunes, Suk-Bong Ha, Neera Tewari-Singh, Kevin J. Morey, Anna M. Trofka, Paul Kugrens, Michael Deyholos, and June I. Medford. A synthetic de-greening gene circuit provides a reporting system that is remotely detectable and has a re-set capacity. *Plant Biotechnology Journal*, 4:605–622, 2006.
- [2] Scott D. Brown and Neik Sanders. *The DIRSIG User’s Manual*. Chester F. Carlson Center for Imaging Science at Rochester Institute of Technology, 54 Lomb Memorial Drive, Rochester, NY 14623-5604, 2007.
- [3] Thomas G. Chrien, Christopher Chovit, and Peter J. Miller. Imaging spectrometer using a liquid crystal tunable filter. *Proceedings of SPIE*, 1937:256–261, 1993.
- [4] Richard O. Duda, Peter E. Hart, and David G. Stork. *Pattern Classification*. John Wiley and Sons, Inc, second edition, 2001.
- [5] David C. Hatchell. *ASD Technical Guide*. Analytical Spectral Devices, Inc., 5335 Sterling Drive, Suite A, Boulder, CO 80301, USA, 3rd ed. edition, 1999.

- [6] Terrence H. Hemmer. Lessons learned in the post-processing of field spectro-radiometric data covering the 0.4 to 2.5 μm wavelength region. *Proceedings of SPIE*, 4049:249–260, 2000.
- [7] Petr Hlubina. Low-coherence spectral interferometry with a michelson interferometer applied to a dispersion measurement of a two-mode optical fiber. In Miroslav Hrabovsky, Pavel Tomanek, and Miroslav Miler, editors, *Proceedings of SPIE*, volume 4016, pages 8–13. SPIE, 2000.
- [8] John F. Huth. History and background of acousto-optical tunable filters (aotfs) for imagery intelligence applications. *Proceedings of SPIE*, 3584:136–141, 1999.
- [9] Emmett J. Ientilucci and Scott D. Brown. Advances in wide-area hyperspectral image simulation. In Wendell R. Watkins, Dieter Clement, and William R. Reynolds, editors, *Proceedings of SPIE*, volume 5075, pages 110–121. SPIE, 2003.
- [10] Photon Systems Instruments. PSI FluorCam, May 2009. <http://psi.cz/products/fluorcams/>
- [11] C. Neal Stewart Jr., Reginald J. Millwood, Matthew D. Halfhill, Mentewab Ayalew, Vinitha Cardoza, Mitra Kooshki, Gene A. Capelle, Kevin R. Kyle, David Piaseki, Gregory McCrum, and John Di Benedetto. Laser-induced fluorescence imaging and spectroscopy of GFP transgenic plants. *Journal of Fluorescence*, 15(5):697–705, 2005.
- [12] Nirmal Keshava. Angle-based band selection for material identification in hyperspectral processing. In Sylvia S. Shen and Paul E. Lewis, editors, *Proceedings of SPIE*, volume 5093. SPIE, 2003.

- [13] Moon S. Kim, Donald T. Krizek, Craig S. T. Daughtry, James E. McMurtrey, Ravinder Sandhu, Emmett W. Chappelle, Lawrence A. Corp, and Elizabeth M. Middleton. Fluorescence imaging system: Application for the assessment of vegetation stresses. *Proceedings of SPIE*, 2959:1–10, 1997.
- [14] J.W. Kury and R.L. Simpson. Development of non-hazardous explosives for security training and testing (nestt). Internal report, Lawrence Livermore National Laboratory, 1995.
- [15] Hartmut K. Lichtenthaler and Joseph A. Miede. Fluorescence imaging as a diagnostic tool for plant stress. *Trends in Plant Science*, 2(8):316–320, 1997.
- [16] Gennadii G. Matvienko, Anatolii I. Grishin, Olga V. Kharchenko, and Oleg A. Romanovskii. Application of laser-induced fluorescence for remote sensing of vegetation. *Optical Engineering*, 45(5):056201–1–5, 2006.
- [17] Patricia Muller, Xiao-Ping Li, and Krishna K. Niyogi. Non-photochemical quenching. a response to excess light energy. *Plant Physiology*, 125:1558–1566, April 2001.
- [18] John A. Richards and Xiuping Jia. *Remote Sensing Digital Image Analysis*. Springer, third ed., 2006.
- [19] John R. Schott. *Remote Sensing: The Image Chain Approach*. Oxford University Press, New York, second edition, 2007.
- [20] John R. Schott, Scott D. Brown, Rolando V. Raqueno, Harry N. Gross, and Gary Robinson. Advanced synthetic image generation models and its application to multi/hyperspectral algorithm development. *Canadian Journal of Remote Sensing*, 15:99–111, 1999.

- [21] R. Glenn Sellar and Glenn D. Boreman. Classification of imaging spectrometers for remote sensing applications. *Optical Engineering*, 44(1):013602–1–3, 2005.
- [22] Zhu Shanbing, Tang Minxue, Ji Yiqun, gong Guangbiao, Zhang Ruirui, and Shen Weimin. Optical design of prism-grating-prism imaging spectrometers. In Yunlong Sheng, Yongtian Wang, and Lijang Zeng, editors, *Proceedings of SPIE*, volume 7156, pages 1–8. SPIE, 2009.
- [23] Malgorzata Sowinska, Bernard Cunin, Francine Heisel, and Joseph A. Miehe. New UV-A laser-induced fluorescence imaging system for near-field remote sensing of vegetation: characteristics and performances. *Proceedings of SPIE*, 3707:91–102, 1999.
- [24] Kristin-Elke Strackerjan. Modeling of spectral effects of water and soil as a surface contaminants in a high resolution optical image simulation. Master’s thesis, Rochester Institute of Technology, 54 Lomb Memorial Drive, Rochester, NY 14623-5604, July 2006.
- [25] Transportation Security Administration. How to get through the line faster. <http://www.tsa.gov/traveler-information/how-get-through-line-faster>
- [26] P.J. Zarco-Tejada, J.C. Pushnik, S. Dobrowski, and S.L. Ustin. Steady-state chlorophyll a fluorescence detection from canopy derivative reflectance and double-peak red-edge effects. *Remote Sensing of the Environments*, 84:283–294, 2003.

Acknowledgements

I would like to express my appreciation to Dr. Kerekes for taking me on as a graduate student and providing steadfast guidance and advice. I would also like to thank my committee members, Dr. David Messinger and Dr. Carl Salvaggio, for their assistance. Also, many thanks to the CIS staff members who helped me along the way. Finally, I offer heartfelt thanks to my parents and my husband for their support.